The Quest for Speed

An Optimal Control Framework for optimizing Speed Skating Technique for Efficiency and Speed across Diverse Conditions

F. van der Veen

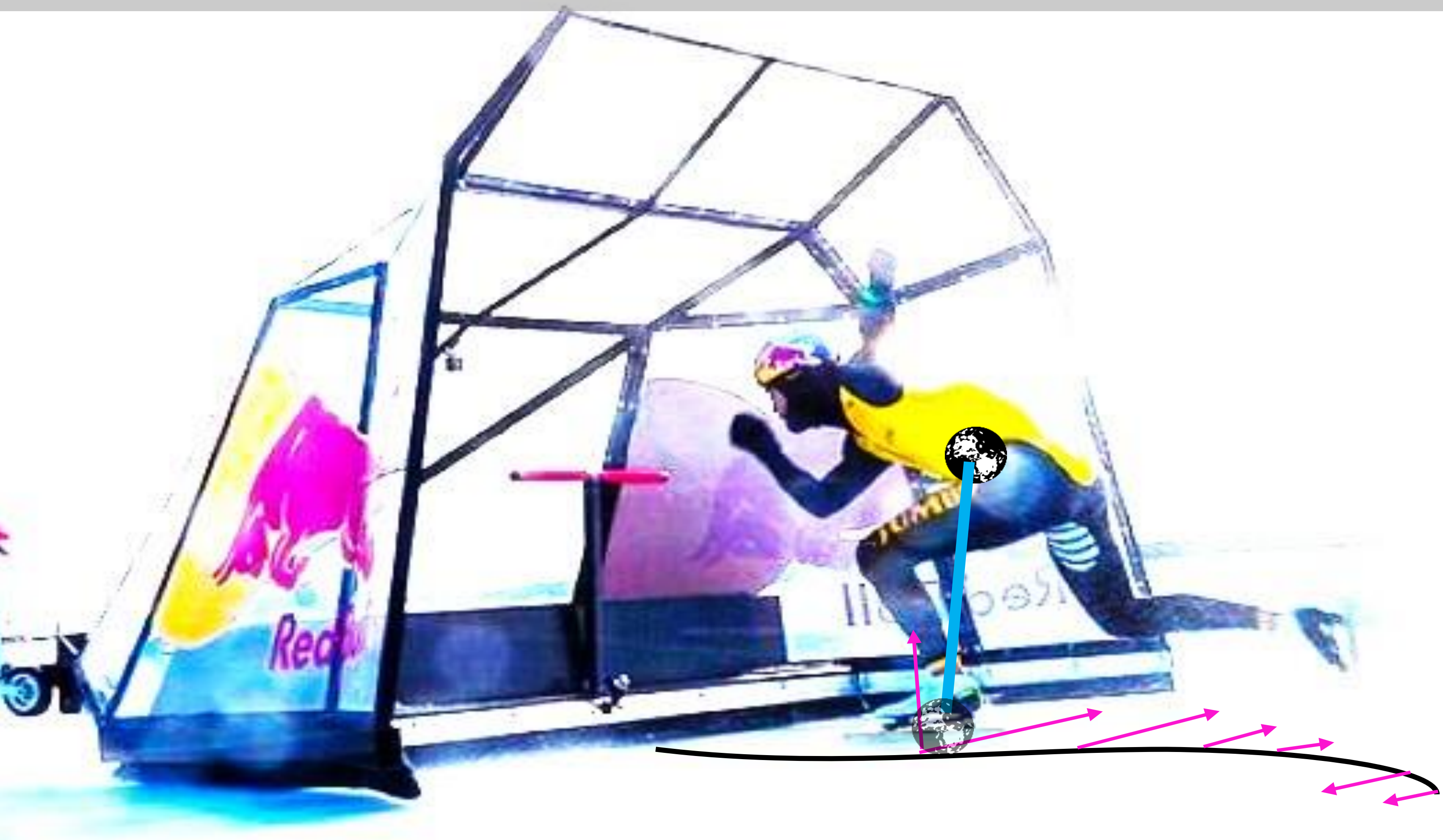

TU Delft Delft University of Technology

The Quest for Speed

An Optimal Control Framework for optimizing Speed Skating Technique for Efficiency and Speed across Diverse Conditions

by

Femke van der Veen

in partial fulfilment of the requirements of Master of Science

in Biomedical Engineering

Track Neuromuscoloskeletal Biomechanics

at the Delft University of Technology,

to be defended publicly on Thursday February 20, 2025 at 10:45 AM.

Student number:	4803914	
Faculty:	Mechanical Engineering (ME)	
Thesis advisors:	Dr. ir. E. Van der Kruk	
	Dr. ir. T. Van Wouwe	
Thesis committee:	Dr. ir. E. Van der Kruk (chair)	TU Delft
	Dr. ir. T. Van Wouwe,	TU Delft
	Prof. dr. F.C.T. van der Helm,	TU Delft
	Dr. J.M. Prendergast,	TU Delft

Cover: Kjeld Nuis in his Quest for speed by Jarno Schurgers (Modified)

TU Delft

The Quest for Speed: An Optimal Control Framework for optimizing Speed Skating Technique for Efficiency and Speed across Diverse Conditions

Abstract—**The optimal technique for individual speed skaters remains poorly understood, due to the complex interplay of technique variables (like stroke frequency, skate trajectory and push-off mechanics). Optimization with a biomechanical model can help to identify the most efficient techniques for individual skaters. This research aimed to use a validated model of a speed skater [1] within an optimization framework to investigate how the optimal speed skating techniques on the straightaways are influenced by individual characteristics and environmental conditions.**

Finding the optimal technique that either minimizes effort at a target velocity or maximizes velocity, was formulated as an optimal control problem and solved using direct collocation. Across different optimizations, stroke frequency, mass, leg length, air and ice friction and limits on average and maximal power were incrementally varied.

Variations in velocity and stroke frequency most clearly influenced the optimal technique. Conditions requiring less energy (optimizations for low velocity, low ice or air friction), optimized towards energy-efficient strokes with longer gliding phases and minimal lateral forces. Conditions with higher speeds and frequencies converged to longer, forceful push-offs. These push-offs maximized leg extension by descending into a deep crouched position to emphasize a sideways push-off. Generally, optimized techniques adapted a small steer angle during the gliding phase to prioritize forward gain, and larger steering angles during the push-off to direct push-off forces forward. Optimizations for higher frequencies adopted more narrow strokes, and reached higher maximized speeds. Regarding personal characteristics, increasing the model's average and maximal power limits most significantly increased maximal velocity.

Index terms—**Biomechanics, sports, optimization, predictive simulation, technique, speed skating**

I. Introduction

In speed skating, the technique is an important factor in reaching peak performance. Elite athletes often attribute underperformance to their technique, describing moments of "missing the stroke" or "failing to translate power into speed" [2], [3]. Previous research has related variations in performance levels to specific differences in push-off mechanics [4]–[6] and has identified factors contributing to differences in speed skating performance [7]–[13]. However, no specific technique could be related to elite speed skaters performing at similar speeds [4], [5]. This suggests that the optimal technique is not universal, but depends on individual characteristics - such as body build and strength - and environmental factors like ice and air friction. [14]. The complex interaction between these factors, combined with the diversity in skaters' body builds, makes it challenging to define the ideal technique in practice. As a result, the optimal technique remains poorly understood. This research aimed to address this gap by exploring how individual and environmental variables influence the optimal speed skating technique by model-based optimizations. In these optimizations, both speed and effort were considered as key performance measures in defining the optimal technique. By focusing on a technique that minimizes effort at a given speed, skaters can maintain higher speeds over longer distances, resulting in improved overall performance.

The speed skating technique is characterized by several components, which could serve as focus areas for coaches and skaters when analyzing and refining the technique. These include:

A. Push-off mechanics

A speed skating stroke involves a gliding and a push-off phase, followed by a repositioning phase [1], [14]. During the gliding phase, the skater balances on one leg, maintaining nearly constant hip and knee angles [7]. During the push-off, the skater is explosively extending the leg to create a push-off force [7], [14], [15]. Longer gliding phase and more explosive push-offs have been associated with higher speeds [7]. The ratio between the horizontal and vertical force components of the push-off force is mainly determined by the lean angle of the skate [10], [16]. Only the horizontal component of the push-off force can effectively contribute to the forward velocity, and therefore an effective push-off places a lot of force in the horizontal direction by a large lean angle [12], [13]. Push-off forces cannot be directed backwards, opposite to the heading direction, due to the low friction of the ice. Consequently, the horizontal push-off forces are primarily directed lateral, perpendicular to the blade [8], [17] to prevent slipping. To be able to convert the lateral forces into forward velocity, skaters steer their skates partly sideways in an angle, so the horizontal force has a forward directed component.

B. Body and skate trajectory

The trajectory of the body plays a role in balance and stroke efficiency. During the gliding phase, the body follows the skate's path to provide balance. The skate is constrained to only glide in the blade's direction.

A crouched position with flexed hip and knee angles minimizes air resistance [4], [10]. Throughout the stroke, the upper body is making a sinusoidal up- and down trajectory. With this pattern, potential energy can be built during the gliding phase and released just before the initiation of the push-off through a passive inwards falling movement of the body towards the opposite lateral direction [4], [10].

As the steer angle of the skate dictates the direction of the lateral push-off force in the horizontal plane [10], [16], the skate's trajectory has a critical role in the force direction. An efficient stroke strikes a balance between gaining maximal forward distance and incorporating enough sideways steering to generate a forward directed force component in the lateral push-off.

C. Stroke frequency

Research showed that speed regulation in speed skating mainly depends on the stroke frequency [4]. However, when looking at speed skaters of the same performance level, speed skating performance could not be related to differences in stroke frequency [4], [8].

Mastering the speed skating technique requires a precise interplay of these technique variables, as even small adjustments in skate trajectory, push-off mechanics, or stroke frequency can significantly affect the skater's overall efficiency and velocity. Experimentally, it is difficult to identify the ideal technique due to the infinite number of possible combinations of these factors, along with individual and environmental variations. Model-based optimization presents a promising alternative [18], due to the potential to tailor the optimization to specific conditions and the possibility to explore extreme cases. In other endurance sports, like swimming, cycling and running, optimizations have provided valuable insights in the optimal techniques [19]–[25]. Although previous studies have explored optimizations for speed skating [14], [26], none have successfully determined the optimal speed skating technique yet. This research used a conceptual, validated model that predicts speed skating behavior on the straights (van der Kruk et al., 2017) [1] for optimizations. This simple model accommodated variations in conditions across optimizations, providing a step toward uncovering broader trends in the optimal skating technique.

The primary aim of this research was to create an optimization framework for speed skating on the straights, to perform model-based optimizations to investigate how individual characteristics (mass, leg length, strength) and environmental factors (air friction, ice friction) influence the optimal speed skating technique in terms of skate trajectory, push-off mechanics, stroke frequency and velocity.

II. Methods

A. Simple Skater Model

The optimization used the three-dimensional (3D) simple skater model (SSM) (van der Kruk et al., 2017) [1]. This model simplifies a skater by two point masses: the center of mass (COM) of the body and the COM of the active skate on the ice, alternating between the left and right skate. Model inputs include the leg extensions (LE), which describe the distance from the COM of the skate to the COM of the body, expressed in the reference frame of the skate (u_s, v_s, w_s), as illustrated in Figure 1. Additional model inputs are the skater's initial position and velocity $(u_b, v_b, w_b, \dot{u_b}, \dot{v_b}, \dot{w_b})$, as well as the skate's steer angle $(\theta_s,)$. The model is further parametrized by the mass (m_{skater}) and ice and air friction coefficients (μ, k). The model distribution coefficient distributes m_{skater} over the point masses of the skate and body. The model outputs, calculated using the TMT method [1], [27], include the updated body positions, velocities and accelerations, and the push-off forces. Leg forces are explicitly modeled (Figure 1). The forces acting on the two point masses are:

$$F = \begin{bmatrix} F_b sin(\theta_b) + F_{leg,x} \\ -F_b cos(\theta_b) + F_{leg,y} \\ -m_b g + F_{leg,z} \\ F_s sin(\theta_s) - F_{leg,x} \\ -F_s cos(\theta_s) - F_{leg,y} \\ -m_s g + F_N - F_{leg,z} \\ M_s \end{bmatrix} \tag{1}$$

In Eq.1, $F_{leg,x}, F_{leg,y}, F_{leg,z}$ are the push-off forces by the leg in x, y and z direction of the global reference frame (N) (Figure 1). F_N is the normal force, $F_b = kv^2$ the air friction working on the body and $F_s = \mu F_N$ the ice friction working on the skate. M_s is a torque to steer the skate, rotating the skate around the $N.y$ axis. θ_b is the body angle relative to the forward direction $(\hat{n}_y)$ and θ_s is the steer angle of the skate.

In the SSM, positions and orientations of the masses can be described in global coordinates ($\mathbf{x} = \begin{bmatrix} x_b & y_b & z_b & x_s & y_s & z_s & \phi_s \end{bmatrix}$) or generalized coordinates $\mathbf{q} = \begin{bmatrix} u_b & v_b & w_b & u_s & v_s & w_s & \theta_s \end{bmatrix}$. The transformation matrix (T) maps generalized coordinates ($\mathbf{q}$) to global coordinates ($\mathbf{x}$):

$$\mathbf{x} = T(\mathbf{q}) \tag{2}$$

This can be used to rewrite the accelerations as:

$$\ddot{\mathbf{x}} = h_{con} + \frac{\partial T}{\partial q}\ddot{q} \tag{3}$$

Where $h_{con} = \frac{\partial^2 T}{\partial q^2}\dot{q}\dot{q}$ is the convective acceleration. The TMT method describes the reduced force matrix ($F_{reduced}$) and reduced mass matrix ($M_{reduced}$) as:

$$M_{reduced} = (\frac{\partial T}{\partial q})^T M \frac{\partial T}{\partial q} \tag{4}$$

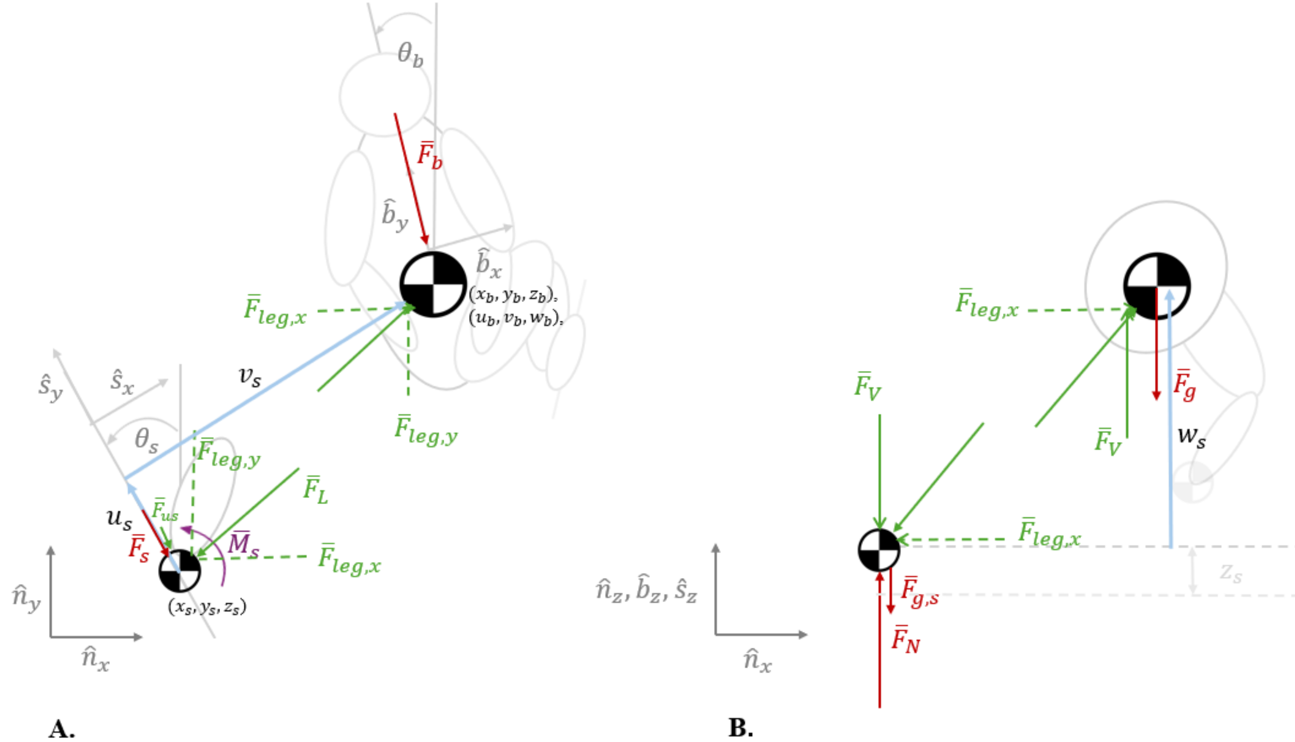

Fig. 1: Free body diagram of the speed skater from a top view (A) and frontal view (B). Indicated are the reference frame of the skater (S) and the body (B) and the global reference frame (N). S and B are rotated counterclockwise by angles θ_s and θ_b around the global z-axis. The leg extension is represented in generalized coordinates u_s, v_s, w_s , indicating the distance from the skate's COM to the body's COM in the S-frame. Acting forces are the push-off forces (in green), friction forces (F_s), normal force (F_N) and gravitational force (F_g). There is a constraint force that prevents lateral slip orthogonal to blade. Adapted from [1]

.

$$F_{reduced} = (\frac{\partial T}{\partial q})^T (F - Mh_{con}) \tag{5}$$

Where M is the mass matrix that contains the masses and inertia of each body, and F is the force matrix with the forces acting on each body (Eq.1), both following the order of $\mathbf{x}$. From equations 3, 4, 5 follows:

$$M_{reduced}\ddot{q} = F_{reduced} \tag{6}$$

A non-holonomic constraint is applied to prevent any lateral movement of the skate orthogonal to the blade (the $\hat{s}_x$ direction, Fig.1.A), to prevent sidewards slip of the skate:

$$v_{skate} \cdot \hat{s}_x = -sin(\theta_s)\dot{y}_s - cos(\theta_s)\dot{x}_s = 0 \tag{7}$$

This non-holonomic constraint will be reorganized as Eq.8 so it can be combined with Eq.6.

$$Ck_{tot}\ddot{q} + Cki = 0, \tag{8}$$

where Ck_{tot} is the Jacobian of the constraints and Cki are the convective acceleration terms of the constraints. Combining Eq.8 and Eq.6 the equations of motion become:

$$\begin{bmatrix} \bar{M}_{red} & Ck_{tot}^T \\ Ck_{tot} & 0 \end{bmatrix} \begin{bmatrix} \ddot{q} \\ \lambda \end{bmatrix} = \begin{bmatrix} \bar{F}_{red} \\ -Cki \end{bmatrix}, \tag{9}$$

where λ is the force that is constraining the lateral motion of the skate. In order to solve this system, Eq. 9 is reorganized in terms of known ($\ddot{q_o}$) and unknown accelerations ($\ddot{q_d}$).

$$\begin{bmatrix} \ddot{q_d} \\ \lambda \end{bmatrix} = \begin{bmatrix} \bar{M}_{dd} & Ck_d^T \\ Ck_d & 0 \end{bmatrix}^{-1} \begin{bmatrix} \bar{F}_d - \bar{M}_{do}\ddot{q}_o \\ -Cki - Ck_o\ddot{q}_o \end{bmatrix} \tag{10}$$

In Eq.10, the unknown accelerations are the accelerations of the body in the horizontal plane: $\ddot{q_d} = \begin{bmatrix} \ddot{u_b} & \ddot{v_b} \end{bmatrix}$. $\ddot{q_o} = \begin{bmatrix} \ddot{u_s} & \ddot{v_s} & \ddot{w_s} & \ddot{\theta_s} & \ddot{w_b} \end{bmatrix}$, when assuming the leg extensions and steer angle accelerations are known, and that the vertical acceleration of the skater COM ($\ddot{w}_b$) is equal to the acceleration of the leg extension ($\ddot{w}_s$). $M_{dd}, M_{do}, F_d, Ck_d, Ck_o$ are the reorganized terms of M, F, Ck_{tot}. The solutions from Eq.10 can be used to calculate the reduced forces on the skate ($\bar{F}_o$).

$$\bar{F}_o = \begin{bmatrix} \bar{M}_{od} & \bar{M}_{oo} & Ck_o^T \end{bmatrix} \begin{bmatrix} \ddot{q_d} \\ \ddot{q_o} \\ \lambda \end{bmatrix} \tag{11}$$

Detailed derivation and explanation of the system dynamics are provided in Appendix A. The SSM dynamics were implemented in Python and validated by comparison to measured data (Appendix B). Key model variables and

Reference Frames	Explanation
N	Global frame (x, y, z)
S	Skate frame
B	Body frame
Coordinates	**Explanation**
x_b, y_b, z_b	COM body global position
u_b, v_b, w_b	COM body generalized coordinates
u_s	Leg extension in S.y direction
v_s	Leg extension in S.x direction
w_s	Height of the COM body mass compared to the COM of the skate
θ_s	Steer angle
θ_b	Body angle
Parameter	**Explanation**
m_{skater}	Skater's body mass
α	Mass distribution coefficient
m_s	Mass distributed in skate COM (αm_{skater})
m_b	Mass distributed in body COM ($(1-\alpha)m_{skater}$)
μ	Ice friction coefficient
k	Air friction coefficient
g	Gravitational acceleration
LE	Leg extension: distance between body and skate ($\sqrt{(u_s^2 + v_s^2 + w_s^2)}$)
LL	Leg length, maximal Euclidean distance COM body to COM skate
Parameter	**Explanation**
F_b, F_s	Air and ice friction force
F_L	Lateral force in skate frame
F_V	Vertical force in skate frame
F_{us}	Longitudinal force in skate frame
$F_{leg,x}, F_{leg,y}, F_{leg,z}$	Leg forces in global x, y, z direction

TABLE I: Explanation of the (generalized) coordinates, constant parameters and outcome measures in the simple speed skater model [1].

parameters are summarized in Table I.

B. Data

The data used for the simulations, optimizations and validations was reused from a previous research (van der Kruk et al., 2017) [1], [26]. The data set included the position, velocity and acceleration data from 23 markers on both the skate and body, captured by a motion capture system, as well as force measurements obtained by a specialized instrumented skates [1], [28]. Each dataset consisted of several strokes on the straights, corresponding to low, medium and high intensity speed skating. From this data, trials from 4 different elite speed skaters were extracted, 2 female and 2 male participants, with masses of 65, 70, 76 and 81 kg. For the optimization of a stroke, data corresponding to one stroke on the left skate was selected. A stroke was defined by the period the measured normal force on the left skate exceeded the normal force on the right skate. The average stroke velocities in the selected strokes ranged between 9 and 13 m/s.

C. Simulated results

For each trial, leg extension over time was calculated from based on positions of the trochanter and foot from the dataset [1], [26]. These leg extensions were used as inputs for forward simulations with the Simple Skater Model in Python to predict forces and body trajectories (Appendix B). The resulting predictions, hereafter referred to as simulated results, were used as a reference for comparing the outcomes of the optimization.

D. Optimization framework

Several optimization scenarios were explored. First, a tracking optimization was performed to validate the optimization framework by matching the simulated results with the optimized data. The aim of the actual optimizations was to identify the optimal skating technique as the technique that requires the *least effort* to cover a distance, with two distinct types of goals:

- Type I: Target velocity
- Type II: Maximize velocity

The average forward velocity (v) of the COM of the body over one stroke was used to define velocity. In different optimizations, stroke frequency (f), mass (m), leg length (LL), air and ice friction coefficients(k, μ) and maximum and average power limits ($P_{max}, Pavg$) were varied in incremental steps (Figure 2).

The problem was formulated as an optimal control problem (OCP) in Python using the open-source optimization tool CASADI [29], [30]. The OCP was expressed as:

$$
\begin{aligned}
\text{Minimize} \quad & J(X, u) && (12)\\
\text{with respect to} \quad & X, u &&\\
\text{subject to} \quad & \dot{X} = f(X, u) && (13)\\
& X_{k+1} = X_k + \dot{X}_{k+1} dt && (14)\\
& x_{\min} \leq X \leq x_{\max}, && (15)\\
& u_{\min} \leq u \leq u_{\max}. && (16)
\end{aligned}
$$

Where the goal was to minimize an objective function $J(X, u)$, with the states (X, representing the body positions) and control inputs (u, representing the leg extensions and steer angle accelerations), subject to the SSM system dynamics $f(X, u)$. The solution space of the state and control variables was bounded by limits, reflecting factors such as kinematic and strength limits, as detailed in section II-G) [31].

The OCP was transformed into a non-linear program (NLP) trough direct collocation with a backward Euler integration scheme, discretizing the states over N = 150 collocation points [30]. A preliminary analysis showed that 150 collocation points gave a good trade-off between accurate optimization results and simulation time (Appendix E). The non-linear problem (Eq.12) was solved by an Interior-Point Method (IPOPT) [32] with maximal 500 iterations and a convergence tolerance of 1e-6. To aid convergence to realistic solutions, averaged simulation results were used as initial guesses for the optimization variables.

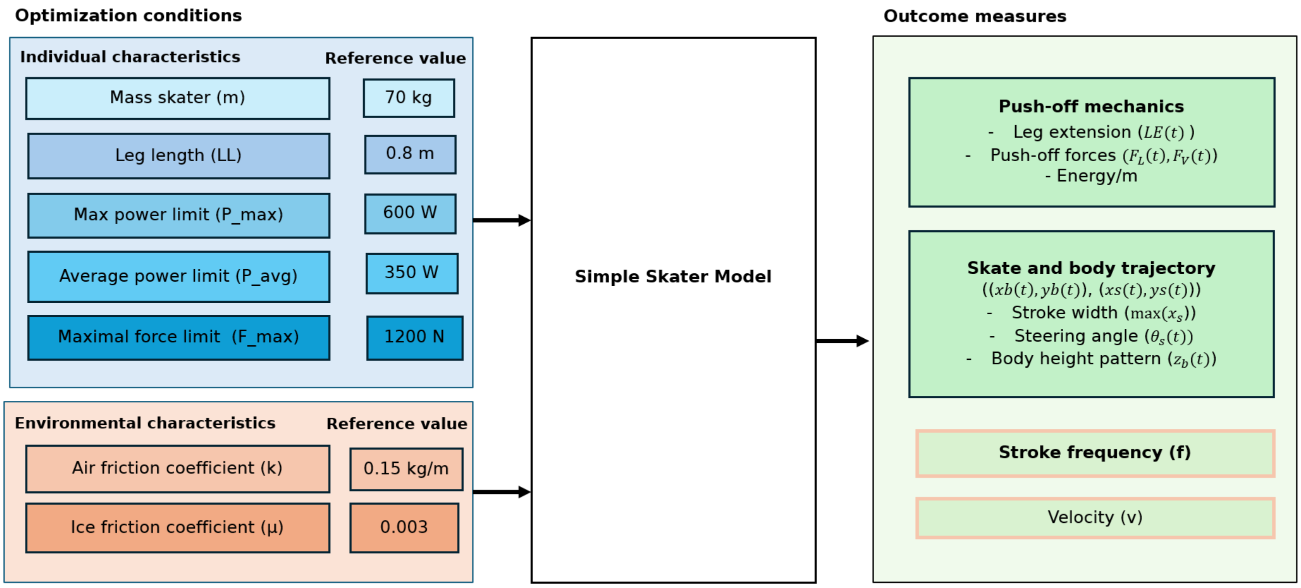

(a)

Optimization TYPE	Varied parameter	Parameter variations	Associated figures TYPE I : Target velocity (v = 8, 10, 12, 14 m/s)	Associated figures Type II : Maximal velocity (v = max)
A	Stroke frequency (f)	0.62, 0.71, 0.83, 1, 1.25, 1.67	3A, B, C; 4, 20	3D, E, F; 19
B	Mass skater (m)	60, 70, 80, 90	18A, 21-24A, 26-29A	6A, 25A, 30A
C	Leg length (LL)	0.65, 0.7, 0.8, 0.9, 0.95	18B, 21-24B, 26-29B	6B, 25B, 30B
D	Max power limit (P_max)	200, 400, 700, 900, 1200	18F, 21-24F, 26-29F	6F, 7, 25F, 30F
E	Average power limit (P_avg)	150, 200, 300, 500, 700	18E, 21-24E, 26-29E	6E, 25E, 30E
F	Air friction coefficient (k)	0.10, 0.13, 0.15, 0.17, 0.20	18C, 21-24C, 26-29C	6C, 25C, 30C
G	Ice friction coefficient (mu)	0.001, 0.003, 0.005, 0.007	18D, 21-24D, 26-29D	6D, 25D, 30D

(b)

Fig. 2: This figure illustrates the optimization framework used in this research. (a) shows the relationship between the optimization conditions and the outcome measures. Each optimization is characterized by its individual characteristics $(m, LL, P_{max}, P_{avg}, F_{max})$ and environmental characteristics (k, μ). Outcomes of the simulations are described in measures for push-off mechanics, trajectory, stroke frequency and velocity. Stroke frequency (f) and velocity (v) are outcomes, but also serve as optimization conditions in case the optimization has to reach a target frequency or velocity. Each optimization (I+II A-G (see (b)) adjusts a parameter in a step-wise way to vary the optimization conditions, while keeping all other parameters constant at their reference values (see (a)). In type I optimizations, target velocities are varied from 8-14 m/s, while in type II optimizations velocity is maximized. With this framework it can be analyze how changes in one parameter affect the optimized results.

E. Optimization scenarios

1) Tracking optimization: Tracking optimizations were performed to validate that the dynamics of the Simple Skater Model [1] were accurately implemented in the CasADi framework. The primary goal was to minimize differences between optimized variables using the optimization framework, and simulated results from the forward simulation with the SSM (section II-C). Instead of directly comparing the optimized variables to measured data, simulated results were used for validation. This ensured that any observed differences were due to differences between the implementation of the optimization framework and the SSM model, and not due to the inability of the model to match measured data, as this has been validated in previous research [1].

The tracking objective function $J(X, u)$ was formulated as the sum of squared differences between both the lateral and vertical skate forces predicted by the optimization $(F_{V,\mathrm{opt}}, F_{V,\mathrm{SSM}})$, and those generated by the SSM model

(F_L, F_V), to align them closely:

$$J = \sum_{k=1}^{N} \Big[(F_{L,\text{opt}}[k] - F_{L,\text{SSM}}[k])^2 + (F_{V,\text{opt}}[k] - F_{V,\text{SSM}}[k])^2 \Big] \tag{17}$$

To quantify if the alignment of the skate forces resulted in an alignment between the inputs and outputs of the optimization framework and SSM model, the Root Mean Square Error (RMSE) was calculated for both the inputs (leg extensions and steer angles) and the outputs (body positions) of the SSM.

$$RMSE_{legext} = \sqrt{\frac{1}{N}\sum_{i=1}^{N}\Big[(u_{s,\text{opt}} - u_s)^2 + (v_{s,\text{opt}} - v_s)^2 + (w_{s,\text{opt}} - w_s)^2\Big]} \tag{18}$$

$$RMSE_{angle} = \sqrt{\frac{1}{N}\sum_{i=1}^{N}\Big[(\theta_{s,\text{opt}} - \theta_s)^2\Big]} \tag{19}$$

$$RMSE_{output} = \sqrt{\frac{1}{N}\sum_{i=1}^{N}\Big[(x_{b,\text{opt}} - x_b)^2 + (y_{b,\text{opt}} - y_b)^2 + (z_{b,\text{opt}} - z_b)^2\Big]} \tag{20}$$

Where $x_{b,\text{opt}}$, $x_{b,\text{opt}}$, $u_{s,\text{opt}}$, et cetera are the results from minimizing the cost function in the optimal control framework, and x_b, y_b, u_b, et cetera are the simulated results (section II-C). For each tracking optimization, initial guesses for body positions, leg extensions, and forces used simulated values. No additional constraints or bounds were applied to the tracking optimization beyond the requirement for the outputs to satisfy system dynamics.

2) Type I: Optimizations to reach a target velocity: As the optimal speed skating technique relies on a balance between speed and effort, understanding the technique that minimizes effort at different velocities (v = 8, 10, 12, and 14 m/s) can offer insights into how skaters can optimize their technique for sprinting or long distance events. The target velocity was defined as the average forward velocity of the body over one stroke (v = mean $\dot{y}_b$). Effort is estimated by the total push-off force over time required to skate a distance. The cost for the effort (J_force) is therefore defined as:

$$J_\text{force} = \sum_{k=0}^{N} F_{tot}[k]dt * N_{strokes} \tag{21}$$

Where $F_{tot}[k]$ is the total push-off force at time [k], including both the lateral and vertical components of the push-off force $(F_L[k], F_V[k])$ and dt the time between collocation points. $\sum_{k=0}^{N} F_{tot}[k]dt$ integrates the total force over time, to compute the total force per stroke [Ns]. $N_{strokes}$ is the number of strokes necessary to complete a distance of 500 m. The final objective for reaching a target velocity with the goal to minimize the effort is (type I):

$$J_I(X,u) = w_1 J_\text{force} + P \tag{22}$$

w_1 weights to what extent larger total leg forces per unit distance are penalized. P includes smoothing terms to prevent sudden peaks in accelerations and tracking terms on the leg extensions to guide the optimization toward realistic speed skating behavior.

3) Type II: Optimizations to maximize skating velocity: In optimizations of type II, the objective promoted higher skating velocities to maximize velocity, by summing the forward velocity ($\dot{y}_b$) over the stroke:

$$J_\text{vel} = \sum_{k=0}^{N} \dot{y}_b[k] \tag{23}$$

Which gives the total objective function:

$$J_{II} = w_1 J_\text{force} - w_2 J_{vel} + P \tag{24}$$

w_1 and w_2 are weight factors that defined the relative importance of the force and velocity costs respectively (J_{force}, J_{vel}).

F. Optimization variations

Initially, optimizations Type I and Type II were performed for different fixed target stroke frequencies (in the range of 0.62-1.67 strokes/s) while keeping individual and environmental parameters constant at their 'reference value'. In this way, solely the impact of stroke frequency on the optimal technique could be explored (optimizations IA and IB, see Figure 2b).

Then, to investigate how the optimal technique changed under different environmental and individual conditions, optimizations were consecutively performed with step-wise changes in the parameters (LL, m, P_{avg}, P_{max}, μ, k), while allowing the stroke frequency to vary between bounds. Each optimization (I+II A-G (see Figure 2b)) incrementally adjusted a parameter, while keeping all other parameters constant at their reference values (Figure 2). LL and m reflect individual characteristics, as do P_{avg}, P_{max}) as a measure of strength. P_{avg}, represents the skater's sustained power output over time while P_{max} reflects the peak power capacity.

G. Constraints

To ensure the optimized skating motion is realistic and repeatable over multiple strokes, several constraints were implemented. An overview of these constraints is provided in Table II. Realistic bounds on the steer angles, leg extensions and body positions, velocities and accelerations were based on the averages and the extremes observed in simulated results from different elite participants (Appendix D). To ensure the leg could not extend beyond the maximal leg length ($LE < LL$), the Euclidean distance between the COM of the body and the COM of the skate ($\sqrt{{u_s}^2 + {v_s}^2 + {w_s}^2}$) was constrained to the leg length.

To make the optimized speed skating motion repeatable across consecutive strokes, final velocities had to match initial velocities in both forward and upward directions to ensure each stroke started with the same velocity. For the lateral movement, initial and final lateral velocities had to be equal in magnitude, but opposite in direction, to reflect the change in direction between strokes on the left and right skate. Additionally, to prevent upward or downward drift after multiple strokes, the final upward body position had to match the initial position.

Furthermore, constraints on the force direction were preventing pulling forces on the ice, either in the lateral or the longitudinal direction.

Limits on $F_{max}, P_{max}, P_{avg}$, should reflect the skater's strength. The power was defined as a gross estimation of the mechanical power, which cannot be compared to other definitions of power [33]. However, it is a good measure to compare power requirements between different techniques. The mechanical power was estimated from the leg extension velocities and forces in the skate plane [14], [15].

$$P = F_V \dot{w}_s + F_{us} \dot{u}_s + kk F_L \dot{v}_s \tag{25}$$

Description	Condition/Bounds
Initial Conditions	
Initial skate position close to COM	$-0.25 < v_s[0] < 0.25$
	$-0.4 < u_s[0] < 0.1$
Minimal initial leg velocity	$-0.5 < \dot{v}_s[0] < 0.5$
	$-0.5 < \dot{u}_s[0] < 0.5$
Initial stroke direction	$\dot{x}_b[0] \geq 0$ (RS), $\dot{x}_b[0] \leq 0$ (LS)
Bounds	
Body position within track	$-3.5 < x_b < 1$ m (if LS)
	$-1 < x_b < 3.5$ m (if RS)
Body height within limits	$0.7(LL + ZS) < z_b < LL + ZS$
Body velocities	$-5 < \dot{x}_b < 5$
	$8 < \dot{y}_b < 18$
	$-1 < \dot{z}_b < 1$
Body accelerations	$-8 < \ddot{x}_b < 8$
	$-8 < \ddot{y}_b < 8$
	$-5 < \ddot{z}_b < 5$
Leg velocities	$-2 < \dot{u}_s, \dot{v}_s, \dot{w}_s, \dot{\theta}_s < 2$
Leg accelerations	$-10 < \ddot{u}_s, \ddot{w}_s < 10$
	$-15 < \ddot{v}_s < 5$
	$-9 < \ddot{\theta}_s < 9$
Stroke duration	$0.6 < T_{\text{stroke}} < 2.0$
Leg extension	$0.5LL < LE = \sqrt{u_s^2 + v_s^2 + w_s^2} < LL$
Body jerk	$\ddot{x}_b[k+1] - \ddot{x}_b[k] < 100$
	$\ddot{y}_b[k+1] - \ddot{y}_b[k] < 100$
	$\ddot{z}_b[k+1] - \ddot{z}_b[k] < 100$
Constraints	
Periodic motion	$z_b[t=0] = z_b[t=\text{end}]$
	$\dot{x}_b[t=0] = -\dot{x}_b[t=\text{end}]$
	$\dot{y}_b[t=0] = \dot{y}_b[t=\text{end}]$
	$\dot{z}_b[t=0] = \dot{z}_b[t=\text{end}]$
	$\ddot{x}_b[t=0] = -\ddot{x}_b[t=\text{end}]$
	$\ddot{y}_b[t=0] = \ddot{y}_b[t=\text{end}]$
	$\ddot{z}_b[t=0] = \ddot{z}_b[t=\text{end}]$
Force limit	$F_{\text{tot}} < F_{\text{lim}}$
Average Power Limit	$P_{\text{avg}} < P_{\text{avg,lim}}$
Power limit	$P_{\text{max}} < P_{\text{max,lim}}$
Prevent pulling force	$F_L v_s \geq 0$ (LS)
	$-F_L v_s \geq 0$ (RS)

TABLE II: Optimization Problem Constraints and Bounds

III. Results

A. Tracking Optimization

The tracking optimization, aimed at matching simulated forces, demonstrated a high degree of alignment between the optimized variables and the simulated model inputs and outputs (Appendix C). The average root mean square error (RSME) for body positions over an entire stroke was 0.0204 ± 0.0025m, indicating an accurate tracking of the skater's trajectory. The RSME for leg extensions was 0.0233 ± 0.0024m, and for steer angles $0.160 \pm 0.021°$. These small errors highlight the capability of the optimization to reproduce the simulated input and outputs values and confirm accurate implementation of the Simple Skater Model (SSM) into the optimization framework.

Therefore, the framework was used to optimize the speed skating technique for various variables at different speeds and stroke frequencies. The technique will be described in terms of stroke frequency, push-off mechanics and the skate and body trajectory.

B. Type I: Optimizations for reaching a target velocity

1) Stroke frequency: When optimizing the technique for different stroke frequencies (OPT IA), a frequency/energy sweet-spot is observed (Figure 3.A). Around a stroke frequency of 1.0 strokes/s, the required energy per meter reaches a minimum, suggesting that each velocity has a stroke frequency that minimizes energy consumption. Increasing or decreasing the stroke frequency beyond this point leads to higher energy requirements. Optimized strokes for lower frequencies are wider and require higher lateral push-off forces/m than more narrow strokes that the optimizer finds for higher frequencies (Figure 3.B+C).

Additionally, optimizations under various conditions (OPT I+II B-G) show that the optimized stroke frequency increases when the model incorporates higher air and ice friction (k, μ), higher velocity (v), and higher average power (P_{avg}). The optimized frequency decreases when mass (m) or leg length (LL) of the model are increased (Appendix F). In optimizations for velocities of 12 m/s and higher, the stroke frequency often converges to the maximum value for all conditions (OPT I+II B-G, Appendix F).

2) Push-off mechanics: When optimizing the skating technique for different stroke frequencies (OPT IA), the model generates distinct lateral push-off force patterns, that align with the energy requirements at different frequencies (Figure 4, Appendix H):

Powerful push-off: For high frequencies (f) the optimization produces a pattern that is characterized by a relatively short gliding phase and longer push-off phase (Figure 4.C). The stroke width is small, and the required lateral forces per meter are relatively low compared to optimized results for lower frequencies (Figure 3.B). However, because the leg extension velocity ($\dot{v}_s$) is high at higher frequencies (Appendix L), energy costs (energy/m) are also relatively high (Figure 3.A, Figure 4).

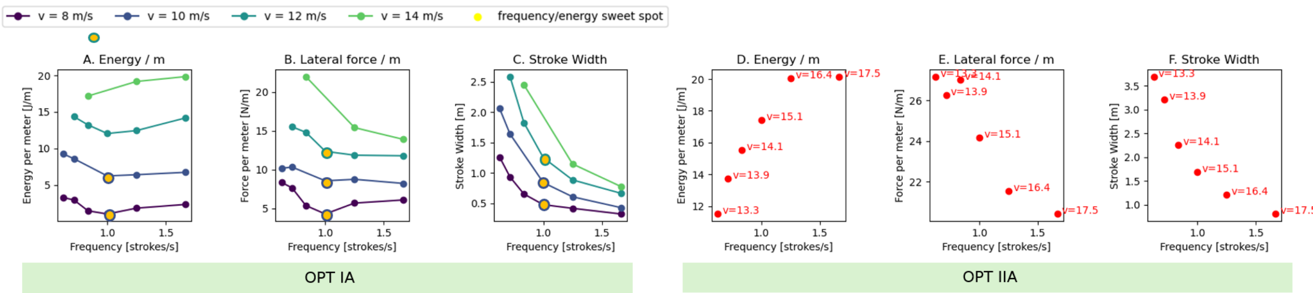

Fig. 3: Effect of varying the stroke frequency (x-axis) on energy per meter, lateral forces, and stroke width across speeds (optimized to reach target velocities (Opt.IA, plots A-C) or to maximize velocity (Opt.IIA, plots D-E)). A frequency of approximately 1.0 strokes/s leads to minimal energy for velocities of 8-12 m/s, the 'frequency/energy sweet spot'. Decreasing stroke frequency leads to wider strokes and higher lateral forces at all velocities. Maximal velocities (red markers) increase with higher stroke frequencies."

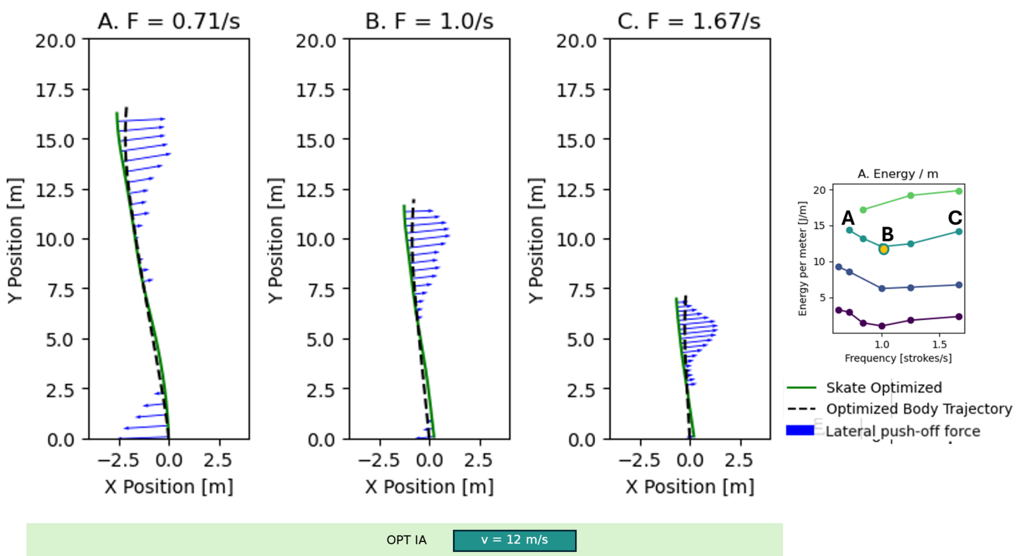

Fig. 4: These plots show the skate and body trajectories in the horizontal plane at a velocity of 12 m/s. The lateral push-off forces are given in blue. At a low frequency (A) the push-off is characterized by a two distinct pushes and a wide stroke. At medium frequency (B) the technique is characterized by a long gliding period. This frequency aligns with the frequency/energy sweet-spot. The push-off at high frequency (C) is characterized by a shorter gliding phase and powerful push.

Extended gliding phase: For optimizations at lower frequencies (f) and lower velocities (v), the model produces a longer gliding phase (Figure 4.B). The energy that is associated with this frequency is around minimal, suggesting a prolonged gliding phase is associated with lower energy expenditure (Figure 3.A).
Second push: At low stroke frequencies, two distinct push-off phases are observed: an initial push at the start of the stroke, which pushes the skate inwards, and a final push-off at the end of the stroke, which pushes the skate sideways (Figure 4.A). As the first push creates a negative directed forward force-component, this push-off is less energy efficient. In the first push, the leg is adducting (v_s is becoming smaller and negative) and then following a 'normal' push-off pattern towards the end of the stroke. The model converges to a starting position that is more parallel to the heading (small θ_s). At low velocities (v = 8, 10 m/s), the optimized push-off pattern include only a minimal initial push-off phase (Appendix H). However, at higher speeds, the model increasingly adopts the second push-off method, even at higher stroke frequencies. As frequency decreases and velocity increases, both the initial and final push-offs become relatively longer with higher push-off forces.

When looking at the push-off mechanics for different conditions (OPT IA-G), the push-off mechanics are primarily influenced by the target velocity (v) of the optimization, as

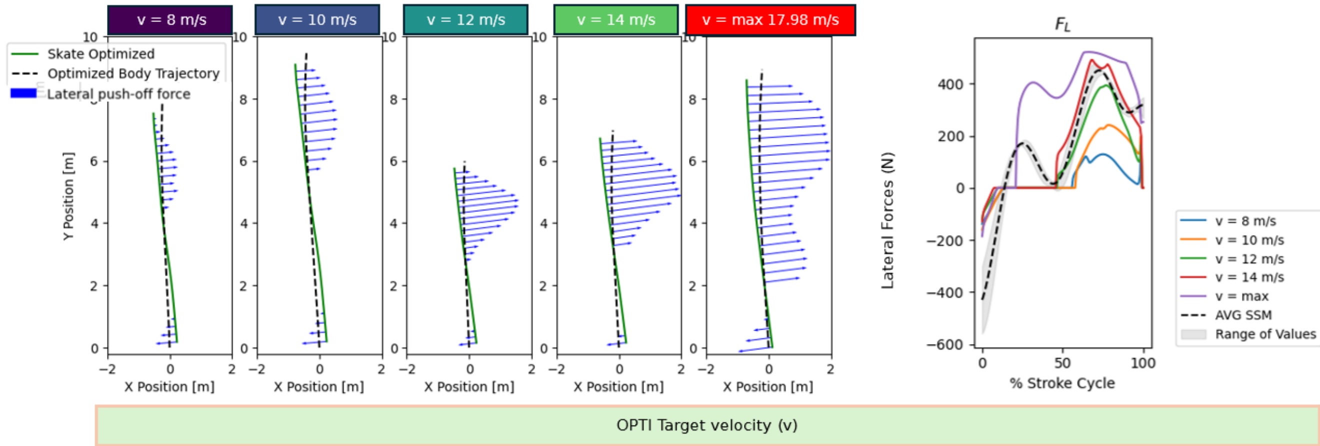

(a) Lateral-push off for different speeds

(b) Lateral forces during the stroke cycle

Fig. 5: This graph illustrates how skating speed influences the optimal lateral push-off patterns. At higher velocities, skaters exhibit relatively shorter gliding phases and earlier push-off onset with larger lateral forces. Plot (A) shows the lateral push-off forces relative to the skate's trajectories for different velocities, while plot (B) depicts these forces across the stroke cycle

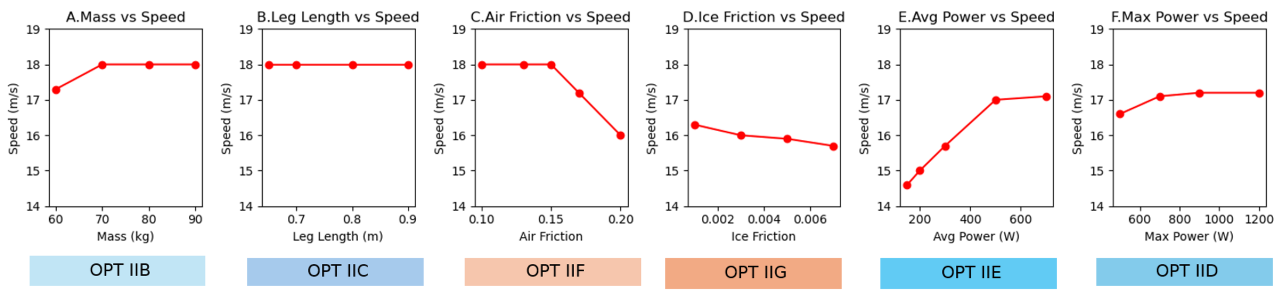

Fig. 6: The influence of individual variables on the optimizations for maximal velocity. Especially power limits and friction influence the maximal velocity. Optimizations with higher friction μ, k reach lower maximal speeds, while optimizations with higher power P_{avg}, P_{max} reach higher maximized speeds.

higher velocities require greater forces due to increased air friction. In conditions with higher target velocities (v), the model compensates with push-off phases that are relatively longer and stronger than for lower velocities (Figure 5.B). When target speeds are increased, the model compensates with a more sideways leg extension pattern ($v_s[t = 100\%]$ is larger) and less backwards ($u_s[t = 100\%]$ is larger) than at lower velocities (Figure 7a.B).

When individual and environmental conditions vary, the optimization adjusts the magnitude for the push-off forces (higher for increasing k, μ, P_{avg}, P_{max} and decreasing m), while the overall push-off pattern remains primarily influenced by velocity (v) (Appendix I).

The optimized push-off mechanics mainly differ from simulated force patterns by a prolonged initial gliding phase with near-zero lateral forces that is not observed in the simulated forces (Figure 5.b)

3) Skate and Body Trajectory: The analysis of the upper body vertical movement at different velocities (v) reveals distinct trends in vertical leg extension w_s (Figure 7a.C). At lower velocities (v = 8-10 m/s), optimized upper body movements (w_s) exhibit larger amplitudes ($\Delta w_s \approx$ 20 cm) of up-and-down movement throughout the stroke cycle. The body falls at an earlier stage and deeper than simulated body movements, resulting in a more pronounced up-and-down motion and higher peaks in the vertical forces. Towards higher velocities (v = 12-14 m/s and maximal velocity), the amplitudes of w_s decreases (Figure 7a.C).

Increasing LL does not change the optimized pattern of w_s, but w_s starts higher at the start of the stroke. A model with higher m, converges to larger up-and down motion at the cost of higher vertical forces F_V. In conditions that increase the required energy (at higher v, μ, k) the optimizations lead to techniques with smaller amplitude of w_s (Appendix I).

The optimized steering angles (θ_s) during the gliding phase are consistently smaller compared to the reference simulated steering angle in all optimization conditions (OPT IA-G, Figure 7a.E), suggesting a focus on gaining forward

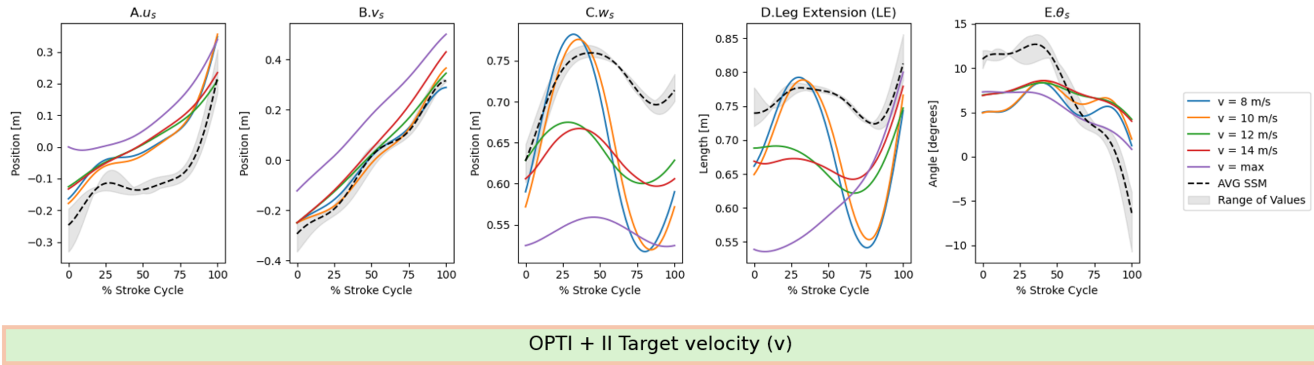

(a) The different push-off mechanics for different velocities. Higher velocities are associated with a more sidewards push off (B, larger v_s) and smaller amplitudes of horizontal body movements (C).

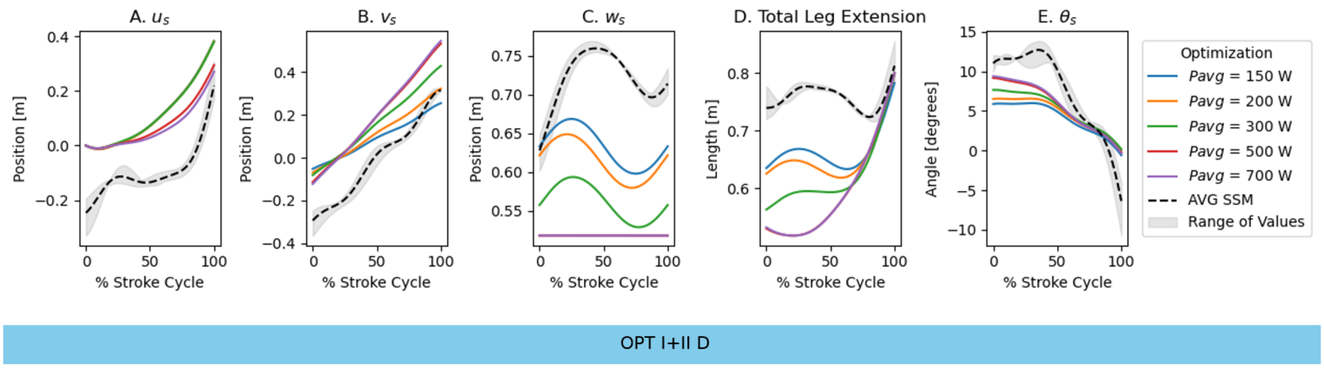

(b) The influence of average power limits on the push-off mechanics. Higher power allows for a larger range of leg extension, by extending the leg further sideways (B, larger v_s), less backways (A, smaller u_s), and starting in a more crouched position (C, smaller w_s). At lower powers the skate is more efficiently gliding forward and less lateral (E, smaller θ_s.

Fig. 7: Push-off mechanics for different situations

distance. In contrast, during the push-off phase, optimized θ_s is larger than simulated θ_s. Optimization conditions with lower P_{avg}, P_{max}, μ, k and v, are associated with a smaller θ_s, particularly during the gliding phase (see also Appendix J). When the model is adapting a low frequency, optimized strokes are wide, and θ_s during the gliding phase is larger.

C. Type II: Optimizations for maximal velocity

The maximal velocities (v_{max}) reached in the optimizations for maximal speed are significantly influenced by changes in the constraint on average power (P_{avg}, OPT IIE, Figure 6.E). Increasing the limit on P_{avg} from 150 W to 200 W steeply raises v_{max} from 14.6 m/s to 15.0 m/s. However, increasing P_{avg} from 500 to 700 W only results in a small increase of v_{max} from 17.0 to 17.1 m/s.

Similarly, when constraints on maximal power (P_{max}) are adjusted in optimizations for maximal speed (OPT IID), increasing P_{max} from 500 W to 700 W raises v_{max} from 16.6 to 17.1 m/s, but further increases have no additional effect on v_{max} (Figure 6.F).

Additionally, optimizations with higher air friction (k) and ice friction (μ) coefficients (OPT IIF+G), converge to a lower v_{max} (Figure 6.C+D). Adapting m and LL in de model (OPT B+C) does not significantly change v_{max}.

1) Stroke frequency at maximal velocity: Optimizations with higher target stroke frequencies (OPT IIA) significantly increase v_{max}. For instance, at f=1.67 strokes per second, a velocity of v_{max}=17.5 m/s is achieved, compared to v_{max}=13.3 m/s at a low frequency of f=0.62 strokes per second (Figure 3.D). For all conditions (OPT IIB-G), optimizing for maximizing velocity results in a maximized frequency (Appendix F).

2) Push-off mechanics at maximal velocity: The techniques optimized for maximal velocity (IIA-G) do not show the long gliding phase that was observed in optimized techniques at lower velocities. Instead, lateral forces (F_L) are higher and persist throughout almost the entire stroke (Figure 5.B). The optimizations for maximal velocity lead to a solution with both v_s and u_s starting near zero, indicating the skate starts close to the body in a more compact position, compared to optimizations for target velocity (v) or simulated results (Figure 7b.A+B).

As previously noted, among individual and environmental conditions, changes in P_{avg} influence v_{max} and push-off mechanics the most. With a lower P_{avg}, the final value of v_s is reduced (0.24 m at 150W vs. 0.54 m at 700W), indicating less sideways lateral leg extension (Figure 7b.B). Consequently, the range of leg extension (LE) during the stroke is smaller, although full leg extension ($LE = LL$) is still reached at the end of the stroke (Figure 7b.D). This occurs because w_s starts at a higher value, reflecting a less crouched position (Figure 7b.C).

3) Skate and Body Trajectory: When maximizing velocity (OPT IIA-G), the model adapts to minimal vertical body movements (Δw_s). The body starts from a low, crouched position (small w_s (Appendix K).

The optimized steer angle (θ_s) during the gliding phase is higher when maximizing speed compared to optimizing for lower target speeds (v) (Figure 7a.E). At v_{max}, the model adapts to a higher θ_s during the gliding phase when optimizing with higher $, P_{avg}, P_{max}$ and smaller θ_s with higher m (Appendix K).

IV. Discussion

This research aimed to create an optimization framework for speed skating to optimize the technique for various individual characteristics, environmental factors, velocity and stroke frequencies to identify trends in the optimized technique.

A key strength was the the wide scope of optimizations performed to explore a range conditions. The results highlighted key factors for making a more efficient and faster stroke by highlighting the impact of stroke frequency, the emergence of different push-off patterns and trends in vertical body movements and steer angle. These findings will be discussed in detail below.

A. Stroke frequency

The results highlighted the central role of stroke frequency in speed skating performance. The optimal stroke frequency that minimizes effort increases with speed, likely due to the increased power required to overcome higher resistances at higher velocities. That explanation aligns with the increased optimal stroke frequency for increased air friction and ice friction coefficients. At high frequencies, the skater can push-off efficiently during the, with many push-offs over time allowing for a high power output over time. In contrast, at lower frequencies, the gliding phase of the stroke dominates and the delayed onset of the lateral push-off forces limits the ability to maintain high velocities. Why the skater cannot give high lateral push-off forces during the whole stroke at low stroke frequencies can be explained as followed. In order to generate forward motion, the leg must extend laterally, propelling the skater forward through the lateral push-off force. However, the length of the leg constrains the range of lateral extension, restricting duration and amount of lateral force that can be applied throughout one stroke. Therefore, it explains why maximized velocities are higher for higher stroke frequencies and why at low frequencies, velocities cannot be maintained as effectively. At lower frequencies, to direct more lateral force in a forward direction, the steering angle must be larger, which leads to a wider stroke and higher lateral forces per meter of distance.

However, skating techniques at higher stroke frequencies at the same velocity demand higher energy, and energy is minimal for lower stroke frequencies (see Figure 3). This trade-off between energy efficiency and performance explains the observed differences in techniques of sprinters and long-distance skaters. Sprinters adopt high stroke frequencies to maximize velocity, while long-distance skater favor lower frequencies to conserve more energy. These findings also align with previous research showing that stroke frequency is a major regulator of speed across different skating distances. [4] These findings imply that sprinters could potentially benefit from a really high frequency to increase their skating speed. However, there is a limit on the maximal stroke frequency. Not only because it requires high power, but also because of physiological constraints. Insights from cycling optimizations demonstrate that in cyclic movements, muscle force decreases at higher frequencies, because of the time-dependent nature of muscle activation and deactivation dynamics. [34]. Furthermore, at high frequencies it can be harder to coordinate the movements and not lose stability.

The optimal stroke frequency tends to decrease with a higher body mass and longer leg length (Appendix F). A higher body mass leads to higher inertia, making it harder to accelerate/decelerate limbs during strokes, therefore favoring a lower frequency compared to a leaner body mass. Longer legs would allow for a longer push-off, so even at a higher speed the slightly lower frequencies can generate enough push-off power to maintain the high speeds. These results align with trends observed in biomechanical studies for other sports, where the optimal cycling cadence decreased with a higher body mass [35]. Another research showed that the optimal cadence decreased with an increasing size of the cyclist [36])

B. Push-off mechanics

Different push-off techniques were observed. The most energy efficient technique was associated with a long gliding phase. It is hypothesized that with this extended gliding phase, forces are reduced to minimize the effort cost in the objective function. This hypothesis is supported by the results of a secondary analysis that showed higher forces when the gliding phase was penalized (Appendix N. The longer gliding phase is in line with a research that showed that elite speed skaters with the same stroke time but better performance, have a longer gliding and shorter push off phase [37]. However, the question is if this optimized technique with a near-zero lateral force during the gliding phase is feasible. It requires the speed skater to be balanced on one leg on the center of the blade. For the speed skater, it is likely hard to balance this way without lateral pressure. It will probably require a lot of corrective muscle forces to keep balance, which are not included in the cost, as the model does not include any muscles. In previous research, longer gliding phases resulted in a reduced blood flow to the muscles, which lead to faster fatigue [10]. Also, the skate cannot be steered as long as there is no lateral force and thus no lean angle, which is now not rightly incorporated in the model (refer to section IV-D).

At high speeds,resistance increases, so the skater has to generate more force during the push off. The strokes are characterized by a longer push-off phase with larger forces and only a short gliding phase. The lateral push off force is showing a similar pattern to the measured forces, with a gradual movement of the leg. A difference in the optimized technique is that the leg is extending further sideways compared to typical observations. In practice, that should correspond to a larger lean angle, which has been associated with faster skating speeds before [7], [13], [37], because more force is applied in horizontal direction.

At low frequencies, the push-off technique starts with a relatively long push on the outside edge of the skate where the skate is abducted with respect to the body COM. This technique is not energy efficient, as the horizontal forces during this push are directed in opposite direction of the movement. A secondary optimization prevented this double push by constraining the lateral forces to be positive (Appendix M). The results showed almost similar total forces and energy over the stroke, and therefore the effort cost is almost equal. However, the technique with the second push is closer to the simulated technique. Therefore, the penalty in the cost function is larger, which might explain why the optimizer is converging to this technique.

C. Body and skate trajectory

Clear differences were observed between the measured and the optimized techniques in terms of steering angle: a smaller angle during the gliding phase and larger angle during the push-off phase in the optimized technique compared to measured angles. During the gliding phase, where the lateral push-off forces are relatively small, the focus is on gaining forward distance and minimizing unnecessary lateral motion to reduce energy losses. During the push-off phase, where the skaters apply the strongest lateral push-off forces, the optimal steering angle is larger then for the measured values. A larger steering angle allows the skater to project the forces more in a forward direction, which can contribute more to forward motion. In situations where less push-off forces are needed or available, with lower velocities, friction, or power limits, the optimal steer angle in the gliding phase is even smaller. When more force is needed, for example for maximizing speed, the steering angle increases.

In the traditional upper body movement, the body is rising during the gliding phase until it starts passively falling just before the push off phase. In the optimized movement patterns at low velocities (8-10 m/s), the body rises during the gliding phase, but descents deeper. This deep descent observed allows for a greater range of leg extension during the push-off phase, as the deeper body position enables the leg to extend more effectively both sideways and backwards. This aligns with findings from prior research, which concluded that smaller pre-extension knee angles are associated with better performance levels [4], [38], as the generated push-off forces mainly come from the extension of the knee [10]. However, this approach requires significantly higher power at the end of the stroke, leading to higher peak power demands. Additionally, maintaining such a crouched position, which is deeper than the height observed in real-world measurements, may increase muscle deoxygenation and lead to fatigue [10], although these effects are not included in the model.

The optimization framework effectively increased speed by identifying techniques that maximized performance, reaching speeds comparable to those of world-class speed skaters. The most decisive factors for achieving maximal speed were increasing average power and, subsequently, maximal power. To optimize for high speeds at elevated power levels, the technique required a deep crouched position, minimal upper body movement, and an explosive leg extension that stretched far sideways and then pushed forcefully backwards.

D. Limitations

1) Model simplification: The model in this study was based on a simplified representation of speed skating trough two connected point masses. The simplicity of the model facilitated computational efficiency, and therefore allowed for the exploration of the technique under a wide range of individual and environmental variables at different velocities.Although the simplified model can recognize trends, the simplicity comes with some limitations:
Lack of a musculoskeletal model: The model did not include any muscles or joints, meaning that the muscle effort required to maintain specific body positions or stability could not be assessed. Without joints, the model cannot capture the specific orientation of the knee, hip and ankle, which makes it difficult to assess whether the specific leg configurations are physically feasible within joint range of motion, or if the position might lead to unstable positions. Additionally, the model cannot account for force-length properties, making it challenging to evaluate whether the leg is positioned to generate force effectively. To partially address this limitation, tracking terms for leg extensions, velocities and accelerations of the leg were incorporated in the cost function, to guide the optimized to realistic solution.
Air friction and body height dependency: In speed skating, COM height typically affects the frontal area and thus the air friction coefficient. However, in the SSM, air friction is estimated based on a fixed frontal area, making it independent of COM height.
Lean angle: The lean angle between the skate and ice skate determines the distribution between the horizontal and vertical push-off force components of the push-off force. Because of the absence of ankle and knee joints in the model, the model lacks the information to calculate the lean angle, possibly leading to unrealistic force predictions. For example, zero lateral force should correspond to zero lean angle. When the leg is not exactly centered under the body, this would be biomechanically infeasible, without awkward leg, knee and ankle angles. This limitation highlights the absence

of crucial joint dynamics and lean angle considerations in the model.

2) Power estimation: Another limitation is the definition of power in this optimization. While the forces and power calculated within the SSM are useful for comparing techniques within the context of this framework, they cannot be applied outside it. The model simplifies power estimation, ignoring joint dynamics and relying on forces that do not accurately match measured values.

3) Cost function: The use of tracking terms on leg extensions within the cost function, based on the average behavior of speed skaters, guided the optimizer toward realistic solutions and improves convergence, given the model's simplicity and freedom within the constraints. Although this approach pushes the optimization in a specific direction, the model remains capable of identifying meaningful trends into potential technique improvements. A technique that resembles the current technique, rather than an revolutionary one, offers practical benefits [39]. It enables faster adoption by skaters. Instead of dictating an entirely new movement pattern, the model highlights trends that can inform refinements to existing techniques, making it a valuable tool for incremental improvements rather than a prescription for exact movements.

The weights applied to forces (J_{force}), tracking terms (P), and velocity (J_{vel}) in the cost function influenced the solution and impacted convergence time. The weights were selected after initial optimizations to favor convergence while minimizing the impact on the simulation outcome.

These weights were subjective, a characteristic common to more optimization problems. Additionally, the cost function used total force over a distance as a measure of efficiency. Although power would provide a better estimation of energy efficiency, attempts to incorporate it into the cost function led to poor convergence.

E. Recommendations for future research

To address these limitations, future research should incorporate a detailed (musculo)skeletal model to better estimate movement feasibility and energy costs. Including lean angle dynamics would improve the distribution between lateral and horizontal push-off forces, enhancing the realism of the simulations. More accurate force and power representations would increase the reliability of the optimized techniques. On-ice measurements with different skating techniques could help to validate whether the observed trends in power, forces, and movement patterns are accurate and truly improve performance. Feedback from coaches and skaters would help to assess the practicality and effectiveness of the optimized movements.

V. Conclusion

This research provided an optimization framework that optimized for different conditions at different velocities and different stroke frequencies to detect trends in the optimized technique. In conclusion, the optimal techniques that minimized the effort at a certain velocity (type I) or maximized velocity (type II) showed the following trends in terms of stroke frequency, push-off mechanics and skate trajectory:

- Skating speed and frequency influence the optimal technique the most.
- Higher frequencies lead to higher maximal velocities, at the cost of increased energy. Energy can be minimized by adapting a lower frequency. To maximize velocity, sprinters should therefore adapt high frequencies, whereas long distance skaters should aim for the best trade-off between an energy-efficient stroke frequency and veloctiy.
- To overcome more friction (at higher velocities or in situations with more air/ice friction), a higher stroke frequency is ideal. Longer leg length and higher skater mass decrease optimal stroke frequency.
- Energy efficient strokes are characterized by a long gliding phase. When maximizing velocity the skater should start with the push off straight away with a powerful push-off.
- Optimized techniques emphasize forward gain during gliding phases by small steer angle, and use larger steering angles during push-off phases to direct lateral forces effectively forward.
- Optimized techniques maximize the leg extension range by adapting a crouched position or descending deeply after the gliding phase, to emphasize the sideways extension of the leg during the push-off.
- The maximal velocity can be mainly increased by higher power and thus strength, of the speed skater. Then the skater can adopt a technique where the leg is explosively extended sideways. Increasing average power is more effective in increasing the velocity than increasing peak power.

A. Implications for the speed skaters

As concluded, optimal skating techniques highly depends on available power and athletes' power demands. Skaters should focus on increasing stroke frequency, as this can can increase their velocity. Skaters could focus building the power and endurance needed to sustain higher frequencies efficiently. Given the greater influence of average power over peak power on maximal velocity, endurance training is particularly important. At high speeds, skaters should focus on executing a powerful lateral push-off from a crouched position. Long-distance skaters can improve energy efficiency by adopting a longer gliding phase with a smaller steer angle.

REFERENCES

[1] Eline Van der Kruk, Dirkjan Veeger, Frans van der Helm, and Arend Schwab. Design and verification of a simple 3d dynamic model of speed skating which mimics observed forces and motions. *Journal of Biomechanics*, 64, 2017.

[2] Jasper Boks. Antoinette rijpma-de jong: 'gekapt met alle bullshit', 2022. Accessed: 2024-12-25.

[3] Josta Bosma. Hoe zet je al die kracht om in snelheid op het ijs?, 2021. Accessed: 2024-12-25.

[4] G. van Ingen Schenau Gj Fau de Groot, R. W. de Groot G Fau de Boer, and R. W. de Boer. The control of speed in elite female speed skaters. (0021-9290 (Print)), 1985.

[5] Eline van der Kruk, Marco M. Reijne, Bjorn de Laat, and DirkJan Veeger. Push-off forces in elite short-track speed skating. *Sports Biomechanics*, 18(5):527–538, 2019.

[6] Ruud W de Boer, Paul Schermerhorn, Jan Gademan, Gert de Groot, and Gerrit Jan van Ingen Schenau. Characteristic stroke mechanics of elite and trained male speed skaters. *Journal of Applied Biomechanics*, 2(3):175–185, 1986.

[7] Ruud W de Boer and Kim L Nilsen. The gliding and push-off technique of male and female olympic speed skaters. *Journal of Applied Biomechanics*, 5(2):119–134, 1989.

[8] Ruud W de Boer and Kim L Nilsen. Work per stroke and stroke frequency regulation in olympic speed skating. *Journal of Applied Biomechanics*, 5(2):135–150, 1989.

[9] S. Felser, M. Behrens, S. Fischer, S. Heise, M. Bäumler, R. Salomon, and S. Bruhn. Relationship between strength qualities and short track speed skating performance in young athletes. (1600-0838 (Electronic)), 2015.

[10] Marco Konings, Marije Elferink-Gemser, Inge Stoter, Dirk Meer, Egbert Otten, and Florentina Hettinga. Performance characteristics of long-track speed skaters: A literature review. *Sports Medicine*, 45:505–516, 2015.

[11] Zimeng Liu, Meilin Ding, Masen Zhang, Bing Yu, and Hui Liu. Effects of technique asymmetry on 500 m speed skating performance. *Bioengineering*, 11(9):899, 2024.

[12] Nina Nässén, Hans-Åke Nässén, and Ann-Marie Pendrill. Arcs on speedskating straightaways: forces, energy and angular momentum. *Physics Education*, 58(1):015013, 2022.

[13] D. A. Noordhof, Marco J. M. Foster C Fau Hoozemans, Jos J. Hoozemans Mj Fau de Koning, and J. J. de Koning. Changes in speed skating velocity in relation to push-off effectiveness. (1555-0265 (Print)), 2013.

[14] T. L. Allinger and A. J. Van Den Bogert. Skating technique for the straights, based on the optimization of a simulation model. *Medicine and Science in Sports and Exercise*, 29(2):279–286, 1997.

[15] D. Fintelman, O. Braver, and Arend Schwab. A simple 2-dimensional model of speed skating which mimics observed forces and motions. pages 4–7, 2011.

[16] E. van der Kruk, A. L. Schwab, F. C. T. van der Helm, and H. E. J. Veeger. Getting the angles straight in speed skating: A validation study on an imu filter design to measure the lean angle of the skate on the straights. *Procedia Engineering*, 147:590–595, 2016.

[17] R. W. de Boer, G. J. C. Ettema, H. van Gorkum, G. de Groot, and G. J. van Ingen Schenau. A geometrical model of speed skating the curves. *Journal of Biomechanics*, 21(6):445–450, 1988.

[18] S. A. McErlain-Naylor, M. A. King, and P. J. Felton. A review of forward-dynamics simulation models for predicting optimal technique in maximal effort sporting movements. *Applied Sciences (Switzerland)*, 11(4):1–20, 2021.

[19] R. H. Miller and J. Hamill. Optimal footfall patterns for cost minimization in running. *Journal of Biomechanics*, 48(11):2858–2864, 2015.

[20] R. H. Miller, Joseph Umberger Br Fau Hamill, Graham E. Hamill J Fau Caldwell, and G. E. Caldwell. Evaluation of the minimum energy hypothesis and other potential optimality criteria for human running. (1471-2954 (Electronic)), 2011.

[21] M. Nakashima. Simulation analysis of the effect of trunk undulation on swimming performance in underwater dolphin kick of human. *Journal of Biomechanical Science and Engineering*, 4(1):94–104, 2009.

[22] M. Nakashima, S. Maeda, T. Miwa, and H. Ichikawa. Optimizing simulation of the arm stroke in crawl swimming considering muscle strength characteristics of athlete swimmers. *Journal of Biomechanical Science and Engineering*, 7(2):102–117, 2012.

[23] M. Nakashima and A. Ono. Maximum joint torque dependency of the crawl swimming with optimized arm stroke. *Journal of Biomechanical Science and Engineering*, 9(1), 2014.

[24] G. Schultz and K. Mombaur. Modeling and optimal control of human-like running. *IEEE/ASME Transactions on Mechatronics*, 15(5):783–792, 2010.

[25] A. Zignoli, F. Biral, B. Pellegrini, A. Jinha, W. Herzog, and F. Schena. An optimal control solution to the predictive dynamics of cycling. *Sport Sciences for Health*, 13(2):381–393, 2017.

[26] Eline van der Kruk. Parameter analysis for speed skating performance. 2018.

[27] J. K. Moore. Learn multibody dynamics, 2022. Accessed: 2025-01-03.

[28] E. van der Kruk, O. den Braver, A. L. Schwab, F. C. T. van der Helm, and H. E. J. Veeger. Wireless instrumented klapskates for long-track speed skating. *Sports Engineering*, 19(4):273–281, 2016.

[29] Joel A. E. Andersson, Joris Gillis, Greg Horn, James B. Rawlings, and Moritz Diehl. Casadi: a software framework for nonlinear optimization and optimal control. *Mathematical Programming Computation*, 11(1):1–36, 2019.

[30] Matthew Kelly. An introduction to trajectory optimization: How to do your own direct collocation. *SIAM Review*, 59(4):849–904, 2017.

[31] F. De Groote and A. Falisse. Perspective on musculoskeletal modelling and predictive simulations of human movement to assess the neuromechanics of gait. (1471-2954 (Electronic)), 2021.

[32] Andreas Wächter and Lorenz T. Biegler. On the implementation of an interior-point filter line-search algorithm for large-scale nonlinear programming. *Mathematical Programming*, 106:25–57, 2006.

[33] E. van der Kruk, F. C. T. van der Helm, H. E. J. Veeger, and A. L. Schwab. Power in sports: A literature review on the application, assumptions, and terminology of mechanical power in sport research. *Journal of Biomechanics*, 79:1–14, 2018.

[34] M. F. Bobbert, Arthur J. Casius Lj Fau Van Soest, and A. J. Van Soest. The relationship between pedal force and crank angular velocity in sprint cycling. (1530-0315 (Electronic)), 2016.

[35] G. Palmieri, M. Tiboni, and G. Legnani. Analysis of the upper limitation of the most convenient cadence range in cycling using an equivalent moment based cost function. *MATHEMATICS*, 8(11), 2020.

[36] H. Gonzalez and M. L. Hull. Multivariable optimization of cycling biomechanics. *Journal of Biomechanics*, 22(11-12):1151–1161, 1989.

[37] Dionne A Noordhof, Carl Foster, Marco JM Hoozemans, and Jos J de Koning. The association between changes in speed skating technique and changes in skating velocity. *International journal of sports physiology and performance*, 9(1):68–76, 2014.

[38] C. Foster, A. C. Rundell Kw Fau Snyder, J. Snyder Ac Fau Stray-Gundersen, G. Stray-Gundersen J Fau Kemkers, N. Kemkers G Fau Thometz, J. Thometz N Fau Broker, E. Broker J Fau Knapp, and E. Knapp. Evidence for restricted muscle blood flow during speed skating. (0195-9131 (Print)), 1999.

[39] P. S. Glazier and S. Mehdizadeh. Challenging conventional paradigms in applied sports biomechanics research. *SPORTS MEDICINE*, 49(2):171–176, 2019.

APPENDIX A
DYNAMICS OF THE SIMPLE SPEED SKATER MODEL

A. Global and generalized coordinates

This section describes and derives the equations of motion that characterize the speed skater's dynamics. These equations are largely based on the Simple Speed Skater model [4] that has been validated before. In the model, the skater is described by two point masses: the center of mass (COM) of the body and the COM of the active skate. This active skate is constantly on the ice during the stroke. The double stance phase is neglected. Instead, during the skating motion, the skater is actively changing between the left skate (kk=1) and right skate (kk = -1). The body is rotated by and angle ϕ_b around the z-axis of the global reference frame, while the heading of the skate is described by a rotation ϕ_b around the z-axis of the global reference frame.

The positions and orientation of these masses in the global reference frame (N) are defined by the global coordinates (x) and their velocities ($\dot{x}$), as illustrated in Figure 8):

$$\mathbf{x} = \begin{bmatrix} x_b & y_b & z_b & x_s & y_s & z_s & \phi_s \end{bmatrix} \tag{26}$$

$$\dot{\mathbf{x}} = \begin{bmatrix} \dot{x}_b & \dot{y}_b & \dot{z}_b & \dot{x}_s & \dot{y}_s & \dot{z}_s & \dot{\phi}_s \end{bmatrix} \tag{27}$$

The generalized coordinates (**q**) and generalized speeds ($\dot{\mathbf{q}}$) describe the positions and velocities of the body relative to the skate in terms of leg extension, defined as:

$$\mathbf{q} = \begin{bmatrix} u_b & v_b & w_b & u_s & v_s & w_s & \theta_s \end{bmatrix} \tag{28}$$

$$\dot{\mathbf{q}} = \begin{bmatrix} \dot{u}_b & \dot{v}_b & \dot{w}_b & \dot{u}_s & \dot{v}_s & \dot{w}_s & \dot{\theta}_s \end{bmatrix} \tag{29}$$

The leg extension is a measure for the distance between the point mass position of the body and the skate (see Figure 8). Here, u_s represents the distance from the skate to the body in the heading direction of the skate ($\hat{s}_y$), v_s is the distance in the lateral direction of the skate ($\hat{s}_x$, perpendicular to the heading direction), and w_s specifies the distance

The transformation matrix maps generalized coordinates (**q**) to global coordinates (**x**). This relation is described by the following equations if coordinates (**x**) are expressed in terms of (**q**)

$$\mathbf{x} = \begin{bmatrix} x_b \\ y_b \\ z_b \\ x_s \\ y_s \\ z_s \\ \phi_s \end{bmatrix} = T(\mathbf{q}) = \begin{bmatrix} u_b \\ v_b \\ w_b \\ -kkv_s cos(\theta_s) + u_b + u_s sin(\theta_s) \\ -kkv_s sin(\theta_s) + v_b - u_s cos(\theta_s) \\ w_b - w_s \\ \theta_s \end{bmatrix} \tag{30}$$

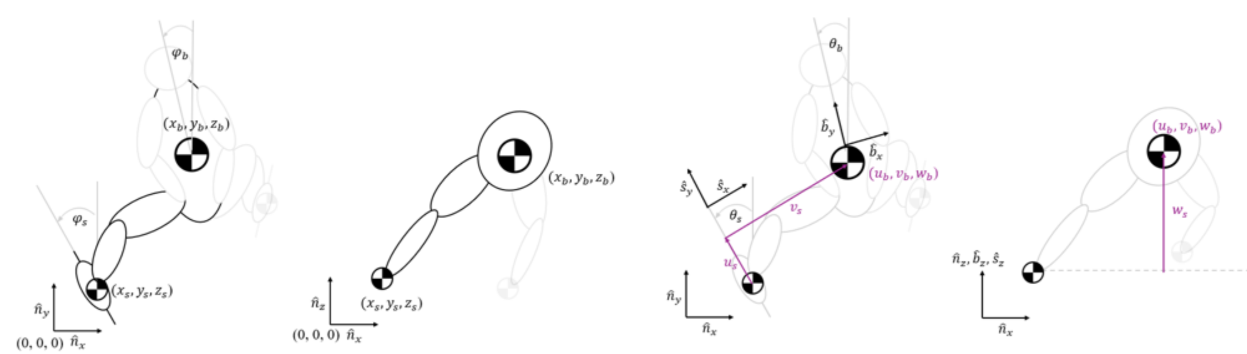

Fig. 8: Description of the model coordinates in global and generalized coordinates (left and right respectively, adapted from: (cite van der kruk 2017)

Expressing the global velocities in terms of generalized coordinates results in the following relation:

$$\dot{\mathbf{x}} = \begin{bmatrix} \dot{x_b} \\ \dot{y_b} \\ \dot{z_b} \\ \dot{x_s} \\ \dot{y_s} \\ \dot{z_s} \\ \dot{\phi_s} \end{bmatrix} = \frac{dT(\mathbf{q})}{dt} = \begin{bmatrix} \dot{u_b} \\ \dot{v_b} \\ \dot{w_b} \\ kkv_s sin(\theta_s)\dot{\theta}_s - kkcos(\theta_s)\dot{v}_s + u_s cos(\theta_s)\dot{\theta}_s + sin(\theta_s)\dot{u}_s + \dot{u}_b \\ -kkv_s cos(\theta_s)\dot{\theta}_s - kksin(\theta_s)\dot{v}_s + u_s sin(\theta_s)\dot{\theta}_s - cos(\theta_s)\dot{u}_s + \dot{v}_b \\ \dot{w}_b - \dot{w}_s \\ \dot{\theta}_s \end{bmatrix} \tag{31}$$

As

$$\dot{x} = \frac{dT(q)}{dt} = \frac{\partial T(q)}{\partial q}\frac{dq}{dt} = \frac{\partial T}{\partial q}\dot{q} \tag{32}$$

Following equation 31 and 32, the expression transformation matrix can be found by using the Jacobian.

$$\frac{\partial T}{\partial q} = \begin{bmatrix} 1 & 0 & 0 & 0 & 0 & 0 & 0 \\ 0 & 1 & 0 & 0 & 0 & 0 & 0 \\ 0 & 0 & 1 & 0 & 0 & 0 & 0 \\ 1 & 0 & 0 & sin(\theta_s) & -kkcos(\theta_s) & 0 & kkv_s sin(\theta_s) + u_s cos(\theta_s) \\ 0 & 1 & 0 & -cos(\theta_s) & -kksin(\theta_s) & 0 & -kkv_s cos(\theta_s) + u_s sin(\theta_s) \\ 0 & 0 & 1 & 0 & 0 & -1 & 0 \\ 0 & 0 & 0 & 0 & 0 & 0 & 1 \end{bmatrix} \tag{33}$$

Looking at the accelerations of global coordinates, these can be reorganized in terms of T as well, using the equation 32 and the chain rule:

$$\ddot{x} = \frac{d}{dt}\dot{x} = \frac{d}{dt}\frac{\partial T}{\partial q}\dot{q} = \frac{d}{dt}(\frac{\partial T}{\partial q})\dot{q} + \frac{\partial T}{\partial q}\ddot{q} = \frac{\partial^2 T}{\partial q^2}\dot{q}\dot{q} + \frac{\partial T}{\partial q}\ddot{q} \tag{34}$$

To simplify the calculations, and isolate the terms for $\ddot{q}$, $\frac{\partial^2 T}{\partial q^2}\dot{q}\dot{q}$ will be called the convective acceleration (h_{con}), so that:

$$\ddot{x} = h_{con} + \frac{\partial T}{\partial q}\ddot{q} \tag{35}$$

This convective acceleration term can be calculated by using the Hessian.

B. Forces

The set contributing external forces to the system are the gravitational force ($F_g = gm_{skater}$) that is working on the body of the skater, and a small gravitational force on the skates, the ice friction force (F_s) that is working on the skate and the air friction force F_b that is working on the body of the skater. The normal force (F_N) is acting on the skate. The internal leg force can be writtenin an x, y, and z component ($F_{legx}, F_{legy}, F_{legz}$

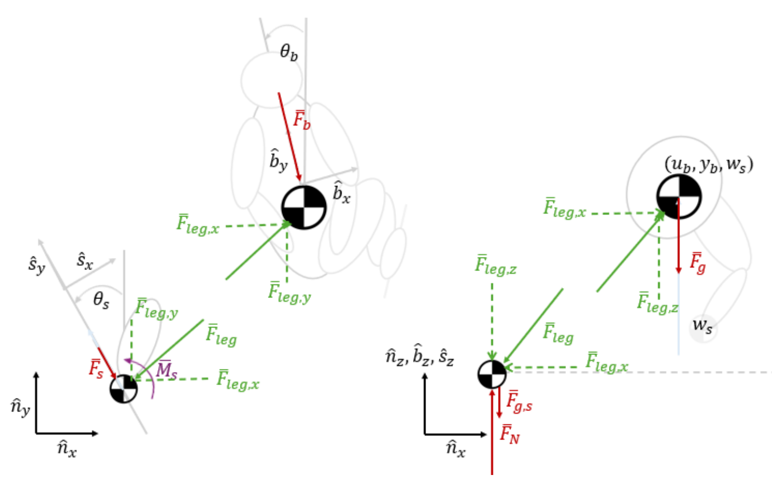

Fig. 9: Internal and external forces working on the COMs of the skate and skater

$$F = \begin{bmatrix} F_b sin(\theta_b) + F_{leg,x} \\ -F_b cos(\theta_b) + F_{leg,y} \\ -m_b g + F_{leg,z} \\ kkF_s sin(\theta_s) - F_{leg,x} \\ -F_s cos(\theta_s) - F_{leg,y} \\ -m_s g + F_n - F_{leg,z} \\ M_s kk \end{bmatrix} = \begin{bmatrix} F_b sin(\theta_b) + F_L cos(\theta_s) \\ -F_b cos(\theta_b) + F_L sin(\theta_s) \\ -m_b g + F_V \\ kkF_s sin(\theta_s) - F_L cos(\theta_s) \\ -F_s cos(\theta_s) - F_L sin(\theta_s) \\ -m_s g + F_n - F_V \\ M_s kk \end{bmatrix} \tag{36}$$

C. TMT Equations of Motion

The masses and inertias from each body can be assembled in a mass matrix (M), that follows the order of the coordinates in x. Generally $F = M\ddot{x}$, so that using equation 31,

$$F = M(h_{con} + \frac{\partial T}{\partial q}\ddot{q}) \rightarrow M\frac{\partial T}{\partial q}\ddot{q} = F - Mh_{con} \rightarrow (\frac{\partial T}{\partial q})^T M \frac{\partial T}{\partial q}\ddot{q} = (\frac{\partial T}{\partial q})^T (F - Mh_{con}) \tag{37}$$

If we now use from the TMT method that,

$$M_{reduced} = (\frac{\partial T}{\partial q})^T M \frac{\partial T}{\partial q} \tag{38}$$

and we call that:

$$F_{reduced} = (\frac{\partial T}{\partial q})^T (F - Mh_{con}) \tag{39}$$

Than from equations 37, 38, 39 it follows that :

$$M_{reduced}\ddot{q} = F_{reduced} \tag{40}$$

1) Non-holonomic constraint: The skate can only glide in the heading direction of the skate. Therefore, the lateral velocity of the skate (in the direction of $\hat{s}_x$ is constrained to be zero. Therefore, the non-holonomic constraint of the system becomes:

$$v_{skate} \cdot \hat{s}_x = -sin(\theta_s)\dot{y}_s - cos(\theta_s)\dot{x}_s = 0 \tag{41}$$

When replacing the global velocities by their expression in generalized speeds (using Eq. 31), the non-holonomic constraint can be expressed as:

$$\begin{aligned} &-(kkv_s sin(\theta_s)\dot{\theta}_s - kkcos(\theta_s)\dot{v}_s + u_s cos(\theta_s)\dot{\theta}_s + sin(\theta_s)\dot{u}_s + \dot{u}_b)cos(\theta_s) - \\ &(-kkv_s cos(\theta_s)\dot{\theta}_s - kksin(\theta_s)\dot{v}_s + u_s sin(\theta_s)\dot{\theta}_s - cos(\theta_s)\dot{u}_s + \dot{v}_b)sin(\theta_s) = 0 \end{aligned} \tag{42}$$

Reorganizing this non-holonomic constraint in terms that are dependent on the accelerations of the global coordinates:

$$Ck_{tot}\ddot{q} + Cki = 0 \tag{43}$$

Therefore, firstly the derivative of the non-holonomic constraint is calculated. Setting all the double derivatives $\ddot{q}$ in this derivative of the non-holonomic constraint to zero, will give you the constraint bias (Ck_i).

$$Ck_i = (sin(\theta_s)\dot{u_b} - cos(\theta_s)\dot{v_b} - \dot{u_s})\dot{\theta}_s \tag{44}$$

The Jacobian of the constraints with respect to $\dot{q}$ can be used to find Ck_{tot}.

$$Ck_{tot} = \begin{bmatrix} -cos(\theta_s) & -sin(\theta_s) & 0 & 0 & kk & 0 & -u_s \end{bmatrix} \tag{45}$$

Adding the non-holonomic constraint, the total equations of motion become:

$$\begin{bmatrix} \bar{M}_{red} & Ck_{tot}^T \\ Ck_{tot} & 0 \end{bmatrix} \begin{bmatrix} \ddot{q}_i \\ \lambda \end{bmatrix} = \begin{bmatrix} \bar{F}_{red} \\ -Cki \end{bmatrix} \tag{46}$$

2) Solving the equations of motion: The equations defined above, will be used to find a solution of the optimization problem. When we assume that the leg extensions, leg extension velocities and accelerations are optimization variables, will serve as the control inputs of the model, so these accelerations will be 'known'. Assuming that during the stroke the skate is staying on the ice, and that therefore the acceleration of the skate is zero, we can assume that the vertical acceleration of the COM of the skater is equal to the acceleration of the leg ($\ddot{w}_s$). The only accelerations that are then unknown are the accelerations of the body in x and y direction ($\ddot{u}_b, \ddot{v}_b$). Therefore, we assume that u_b and v_b are the unknown coordinates ($q_d = [u_b, v_b]$). The generalized coordinates can be reorganized in terms of known coordinates (q_o) and unknown (q_d) coordinates. The generalized speeds and generalized accelerations are the derivatives and double derivatives of these coordinates respectively $\dot{q}_d$ and $\dot{q}_o$. These reorganized coordinates can be used to reorganized the equations of motion, as:

$$\begin{bmatrix} \bar{M}_{dd} & \bar{M}_{do} & Ck_d^T \\ \bar{M}_{od} & \bar{M}_{oo} & Ck_o^T \\ Ck_d & Ck_o & 0 \end{bmatrix} \begin{bmatrix} \ddot{q}_d \\ \ddot{q}_o \\ \lambda \end{bmatrix} = \begin{bmatrix} \bar{F}_d \\ \bar{F}_o \\ -Cki \end{bmatrix} \tag{47}$$

This equation can be solved to find the unknown expressions for $\ddot{q}_d$ and λ:

$$\begin{bmatrix} \ddot{q}_d \\ \lambda \end{bmatrix} = \begin{bmatrix} \bar{M}_{dd} & Ck_d^T \\ Ck_d & 0 \end{bmatrix}^{-1} \begin{bmatrix} \bar{F}_d - \bar{M}_{do}\ddot{q}_o \\ -Cki - Ck_o\ddot{q}_o \end{bmatrix} \tag{48}$$

The solutions from Eq.48 can be used to calculate the reduced unknown forces on the skate ($\bar{F}_o$).

$$\bar{F}_o = \begin{bmatrix} \bar{M}_{od} & \bar{M}_{oo} & Ck_o^T \end{bmatrix} \begin{bmatrix} \ddot{q}_d \\ \ddot{q}_o \\ \lambda \end{bmatrix} \tag{49}$$

These forces are the unknown entries from the reduced force Matrix, which is defined as:

$$\bar{F}_o = \begin{bmatrix} F_N - gm_b - gm_s \\ F_s kk \sin^2(\theta_s) - F_s \sin^2(\theta_s) + F_s - 2m_s\dot{\theta}_s\dot{v}_s + m_s u_s \dot{\theta}_s^{\,2} \\ kk\Big[F_L - \frac{1}{2}(F_s kk \sin(2\theta_s) + F_s \sin(2\theta_s)) + m_s v_s \dot{\theta}_s^{\,2} + 2m_s\dot{\theta}_s\dot{u}_s\Big] \\ -F_N + F_V + gm_s \\ -F_L u_s + \dfrac{1}{2}F_s kk v_s[(-kk+1)\cos 2\theta_s + kk + 1] + \dfrac{1}{2}F_s u_s \sin 2\theta_s[kk-1] + M_s kk \\ \qquad +(kk-1)m_s u_s v_s(\dot{\theta}_s)^2 - 2kkm_s v_s\dot{\theta}_s\dot{v}_s - 2m_s u_s\dot{\theta}_s\dot{u}_s \end{bmatrix} \tag{50}$$

Solving this system, the values for F_L and F_V can be found, which are the push-off forces exerted on the skate in the reference frame of the skate. $F_{leg,x}, F_{leg,y}, F_{leg,z}$ are the forces in the global frame.

$$F_{tot} = \sqrt{F_L^2 + F_V^2} \tag{51}$$

APPENDIX B
SIMULATION RESULTS UPDATED PYTHON SKATER MODEL

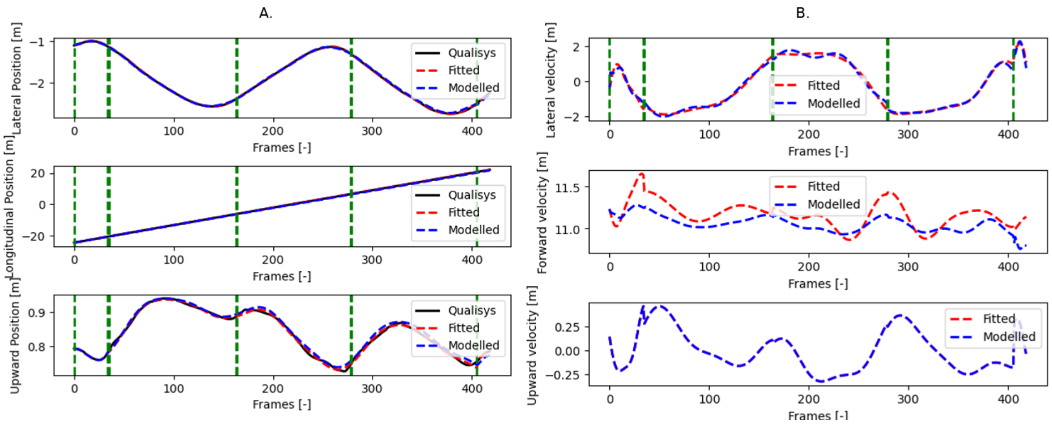

Fig. 10: Simulation results of the body positions (A) and velocities (B) compared to the measured body positions and velocities. The positions and velocities can be predicted quite accurately.

APPENDIX C
RESULTS TRACKING OPTIMIZATION

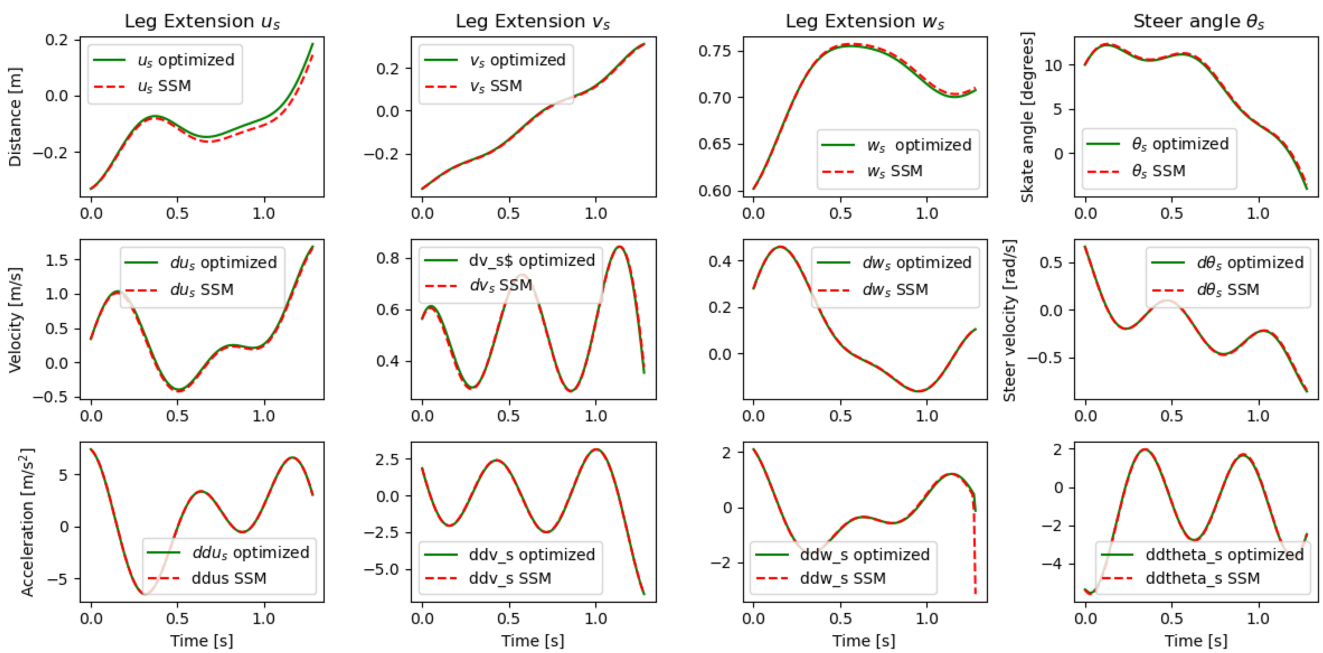

Fig. 11: Example of the results of a tracking simulation, in this case for person P7, Lap Fast 3. The leg extensions can be accurately tracked.

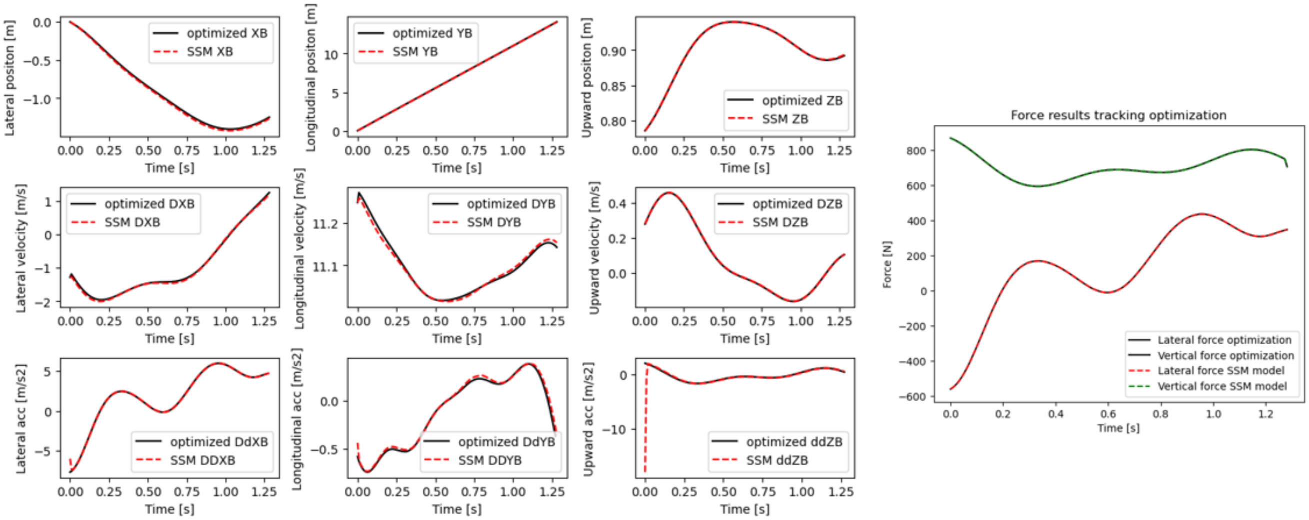

Fig. 12: Tracking results output data from SSM (body positions, velocities and accelerations and forces) over one stroke on the left skate from different trials and the average. When matching the forces, the body positions can be tracked quite accurately.

APPENDIX D
TRACKED DATA

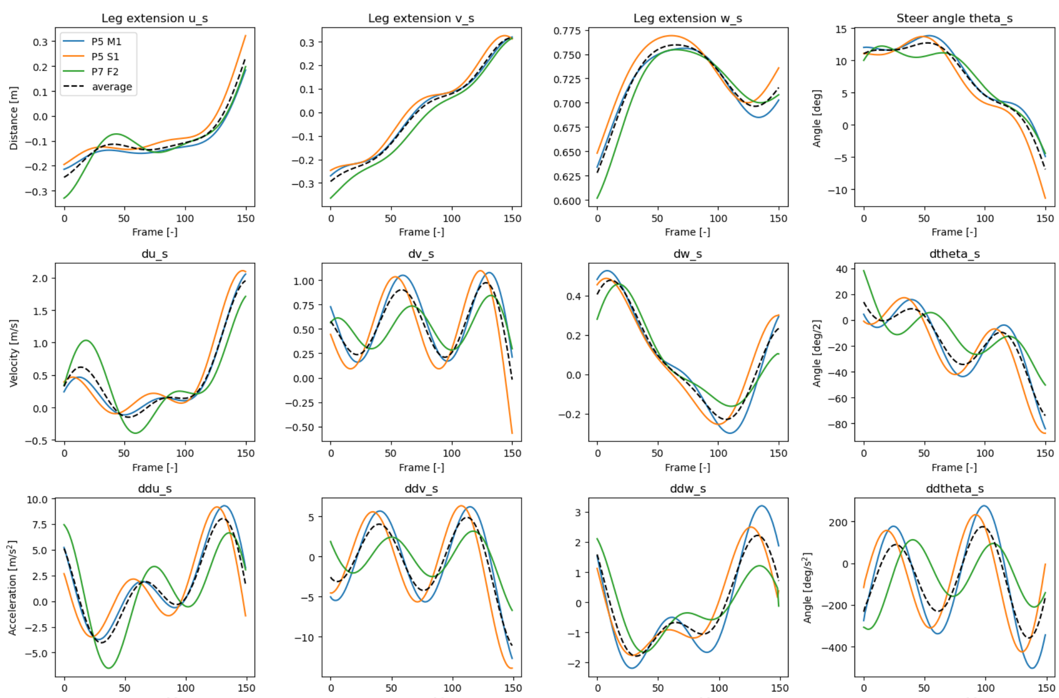

Fig. 13: Tracked input data from SSM (leg extensions) of one stroke on the left skate, from different trials. The average of the trials is given as well.

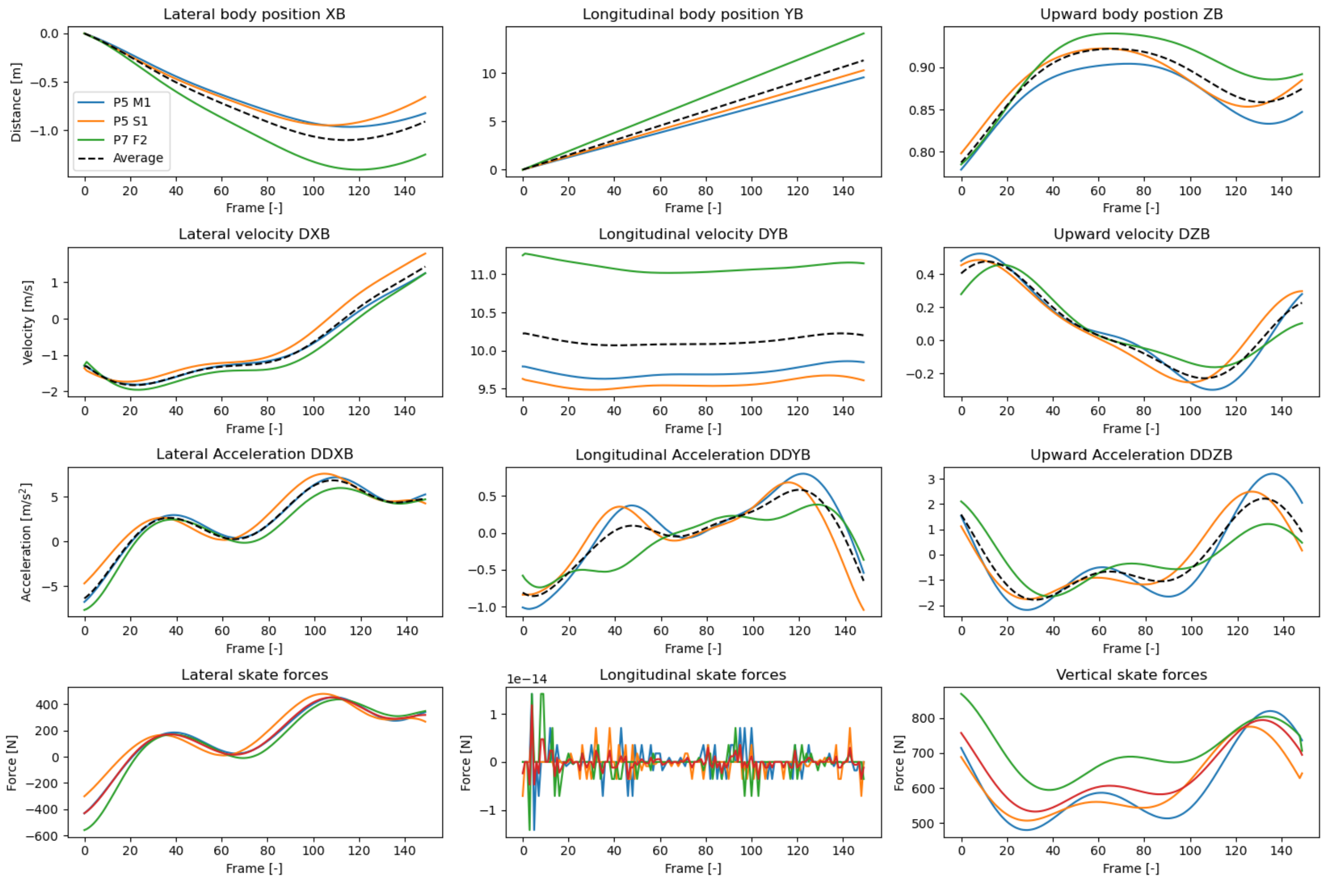

Fig. 14: Tracked output data from SSM (body kinematics and skate forces) over one stroke on the left skate from different trials and the average

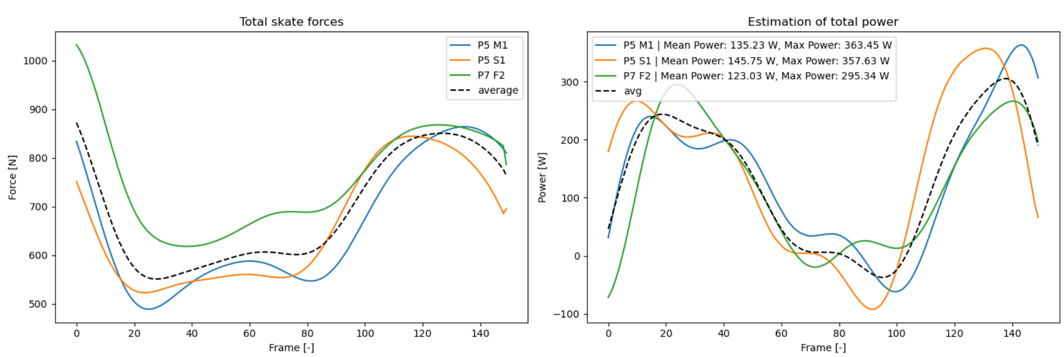

Fig. 15: Tracked output data from SSM (Total force and estimation of the power) over one stroke on the left skate from different trials

Appendix E
Number of collocation points

Increasing the number of collocation points will improve the accuracy of the optimization results. However, increasing the number of derivatives that needs to be calculated, and therefore the calculation time is increased. Therefore, the goal is to find a minimal number of collocation points that can give an accurate result.

A. Methods

Tracking optimizations were performed using different number of collocation points (50, 100, 150, 200, 250 and 300). The accuracy of the output (the body positions) of the tracking simulation is calculated based on the root mean square error

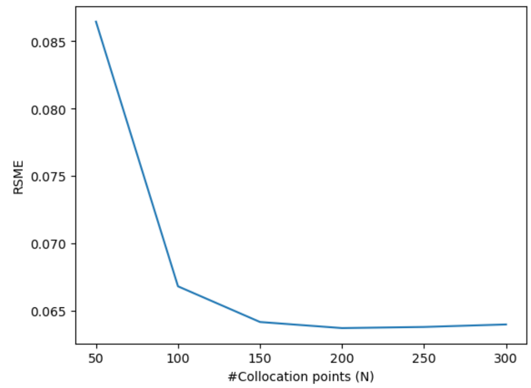

Fig. 16: The relation between the number of collocation points in the optimization and the root mean squared error (RSME) of the body positions

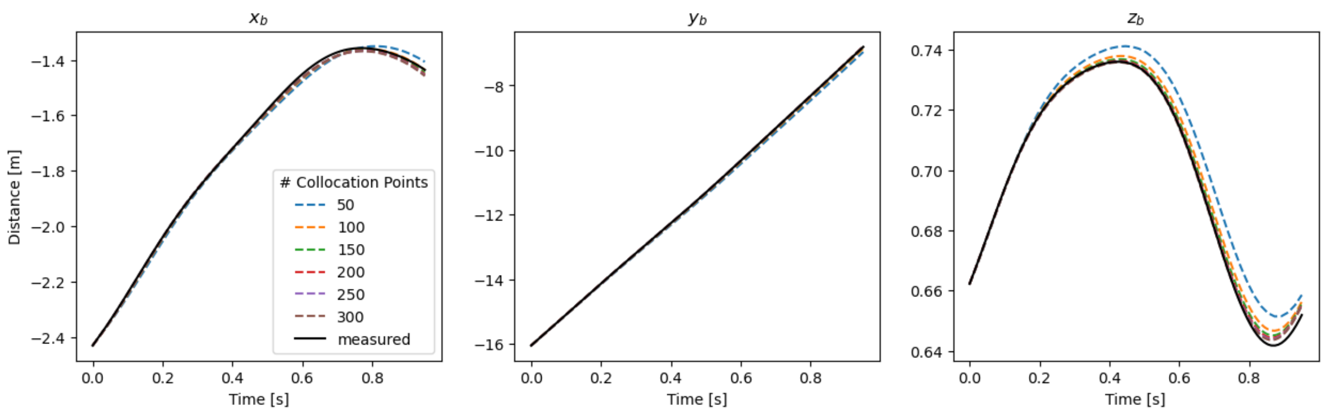

Fig. 17: The relation between the number of collocation points and the optimized body positions (x_b, y_b, z_b)

(RMSE (Eq.52). This RMSE gives a measure of the differences between the optimized body positions and the simulated body positions.

$$\text{RMSE} = \sqrt{\frac{1}{N}\sum_{i=1}^{N}\left[(x_{b,\text{opt}} - x_b)^2 + (y_{b,\text{opt}} - y_b)^2 + (z_{b,\text{opt}} - z_b)^2)\right]} \tag{52}$$

B. Results

The relation between the number of collocation points and the RMSE is given in Figure 16. The resulting impact on the estimation of the body positions is given in Figure 17.

C. Conclusion

Using 150 collocation points will give a good trade-off between the cost of calculation and the accuracy of the optimization results.

Appendix F
Optimized frequencies for different variables

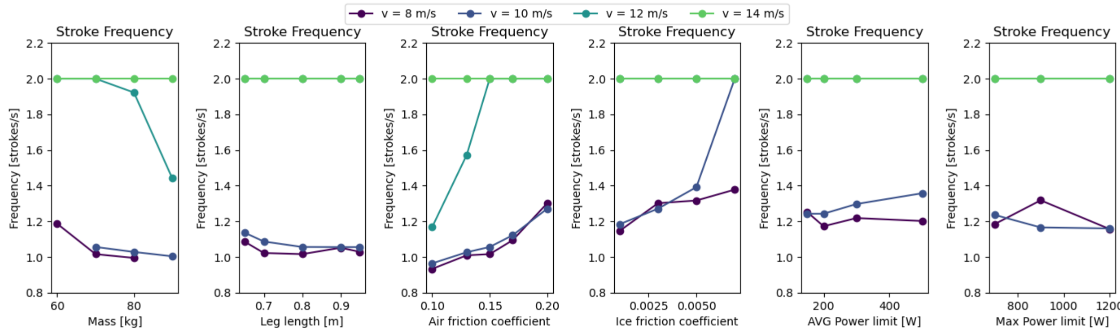

Fig. 18: Optimized frequencies when optimizing the technique to reach target speeds (type I). Increasing speed leads to higher optimal stroke frequencies. Stroke frequency is maximal for higher speeds (12- 14 m/s across variables). Higher air and ice friction increase the optimal stroke frequency, whereas mass and leg length decrease the optimal stroke frequency.

Appendix G
Stroke Trajectories for different stroke frequencies at MAXIMAL speed

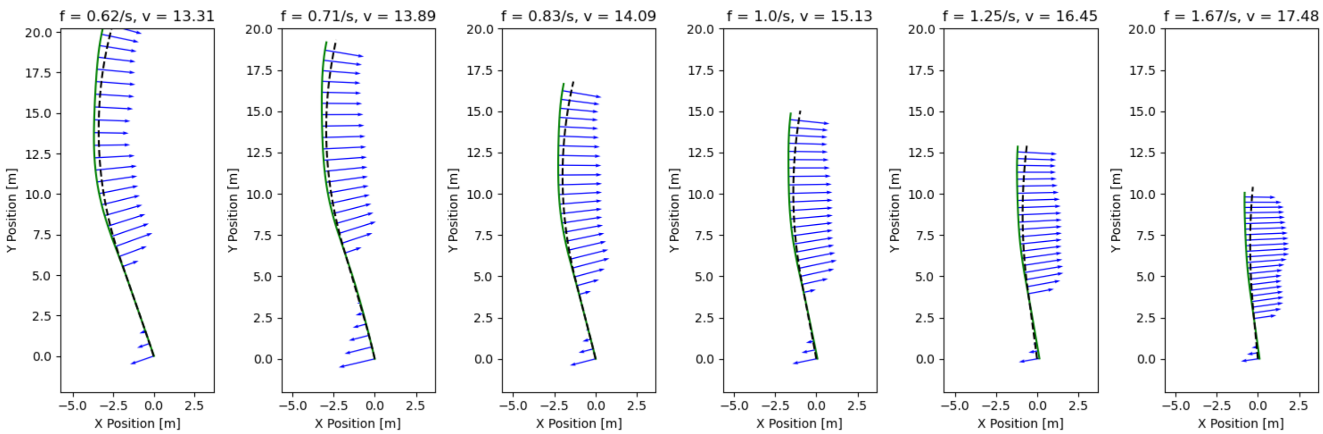

Fig. 19: Stroke trajectories and lateral push off forces for different target stroke frequencies at maximal speed

APPENDIX H
STROKE TRAJECTORIES FOR DIFFERENT TARGET FREQUENCIES

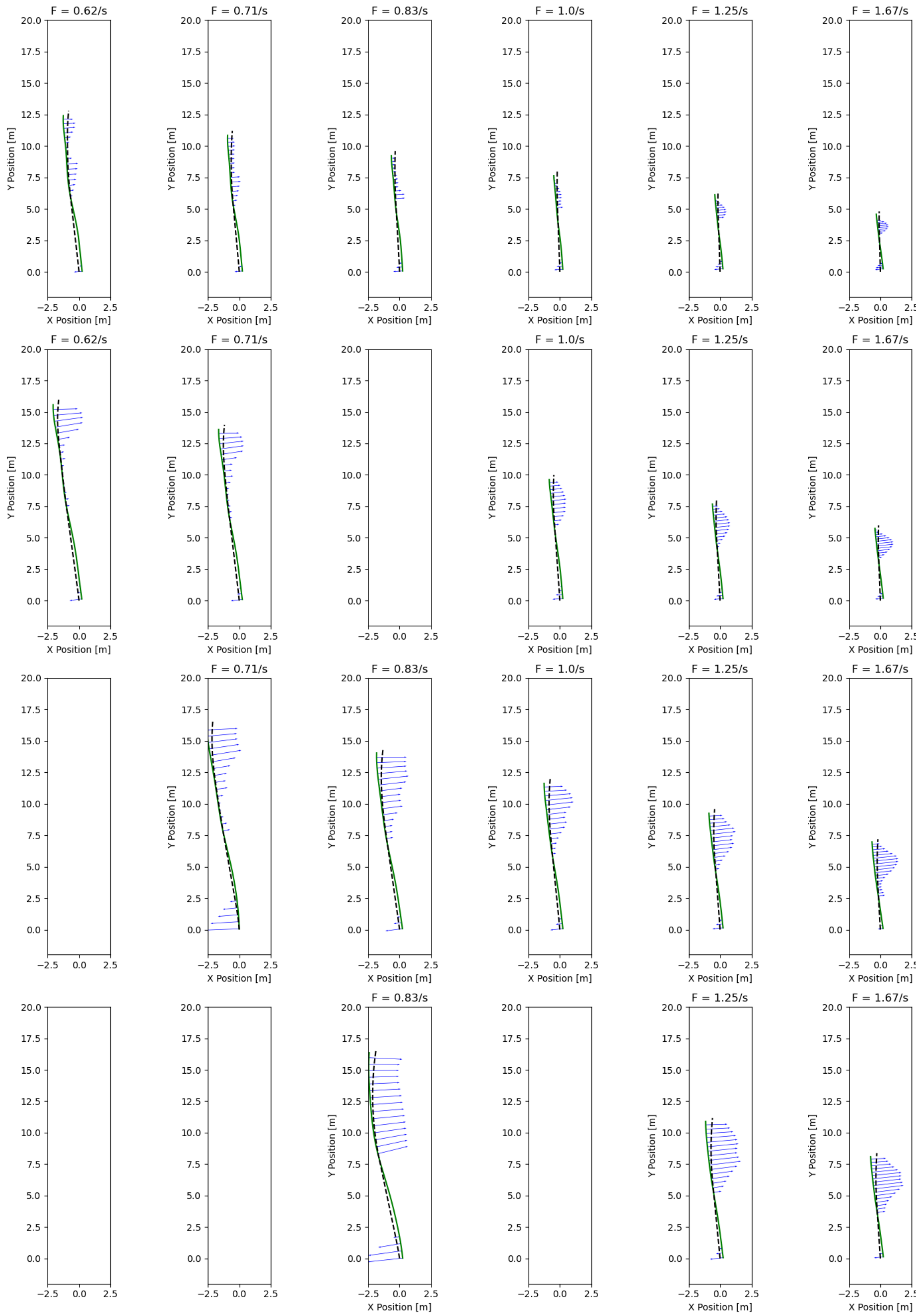

Fig. 20: Stroke trajectories for different target stroke frequencies, where each row represents a different target speed: 8 m/s, 10 m/s, 12 m/s and 14 m/s

APPENDIX I
TRAJECTORIES AT DIFFERENT TARGETS SPEEDS

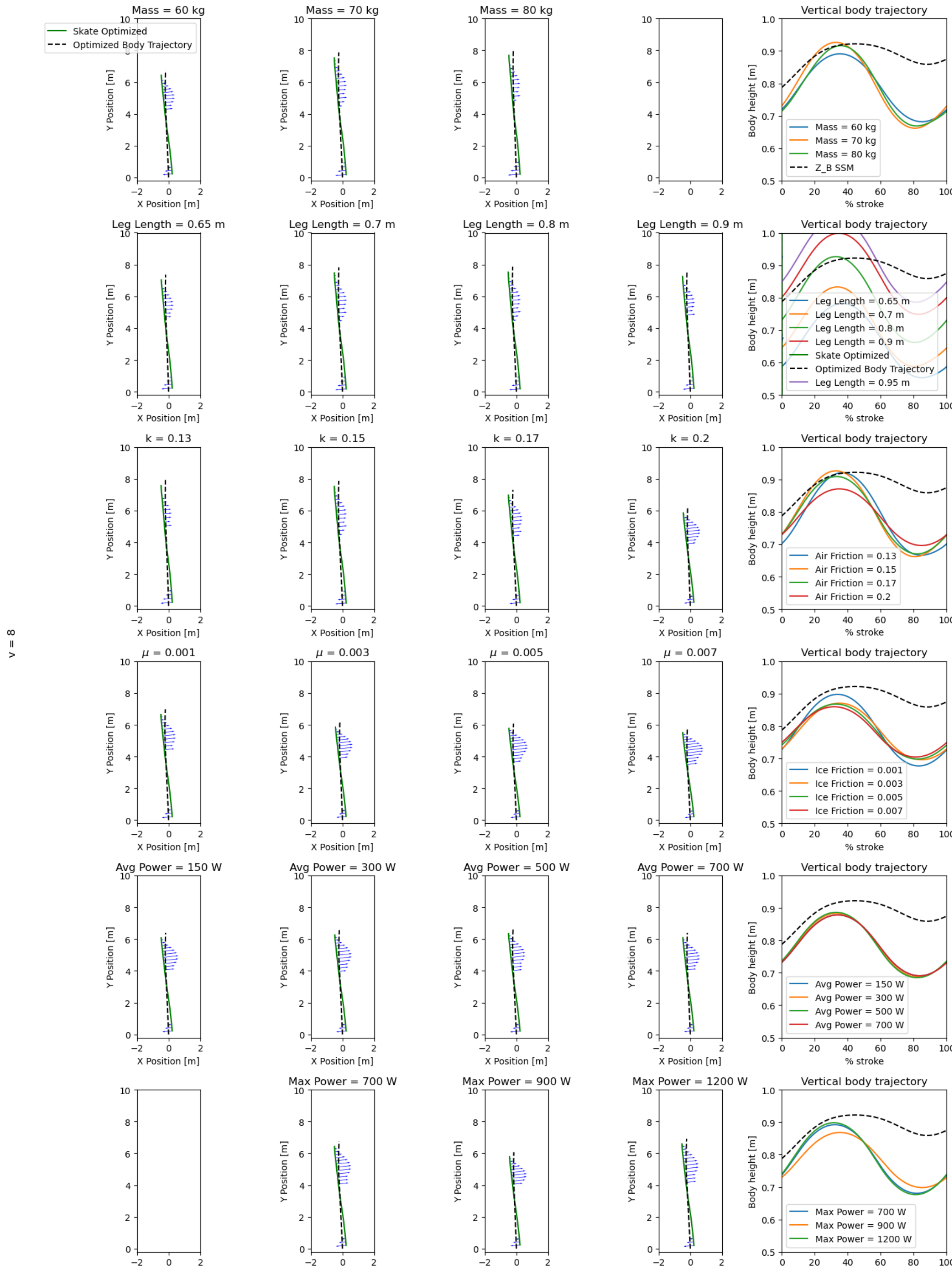

Fig. 21: Results of the optimized trajectories and lateral force for different variables at a speed of 8 m/s

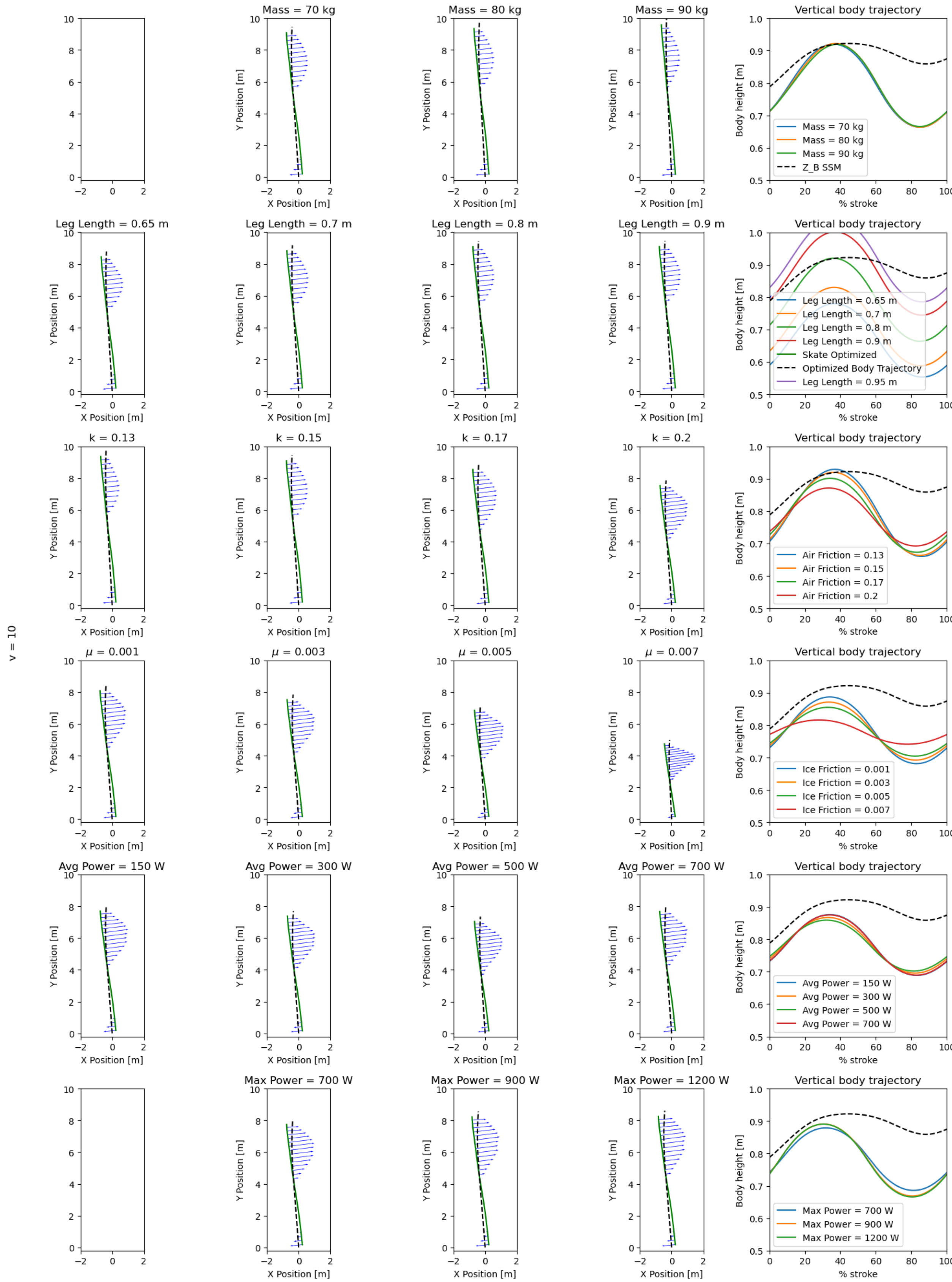

Fig. 22: Results of the optimized trajectories and lateral force for different variables at a speed of 10 m/s

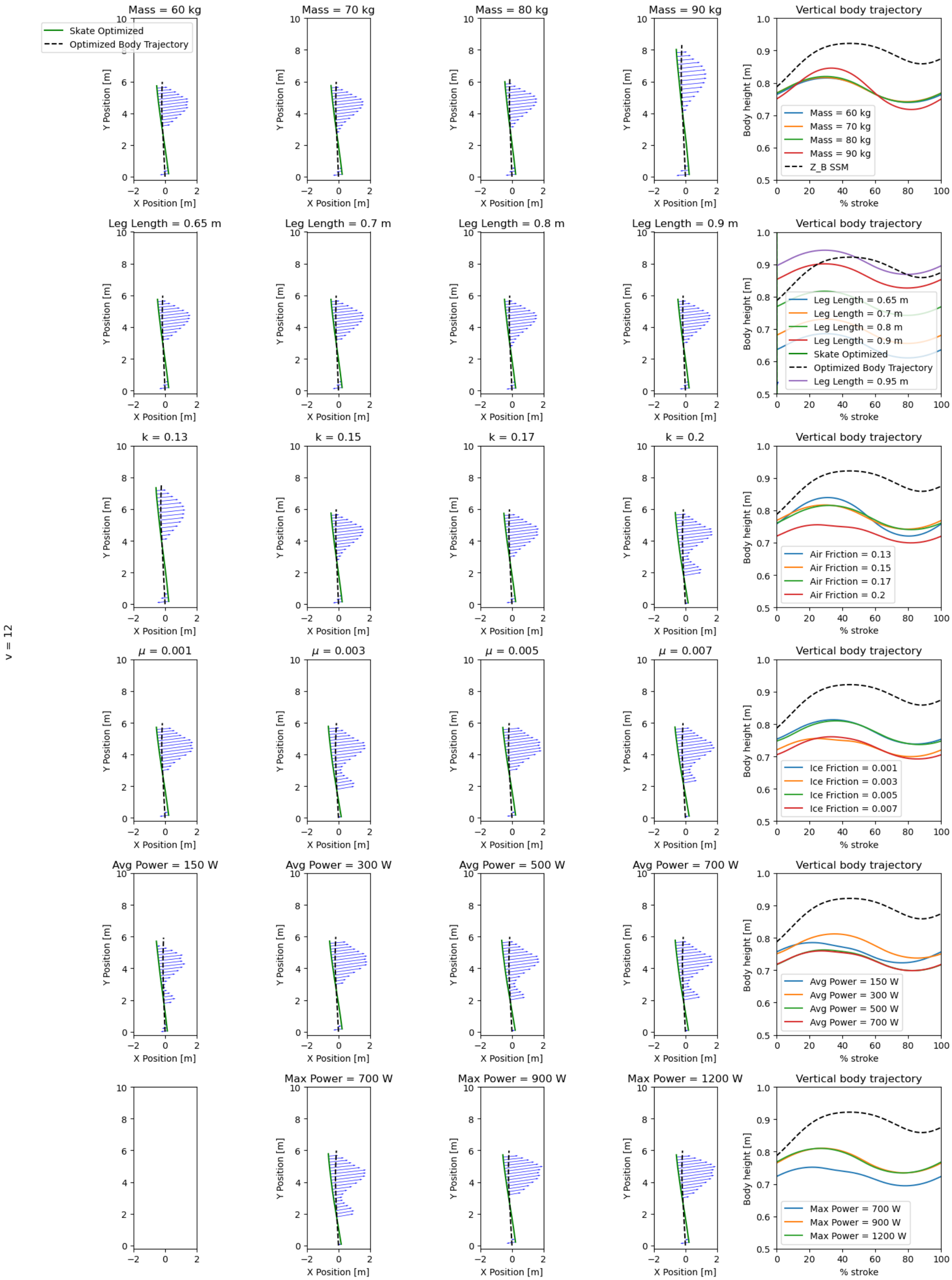

Fig. 23: Results of the optimized trajectories and lateral force for different variables at a speed of 12 m/s

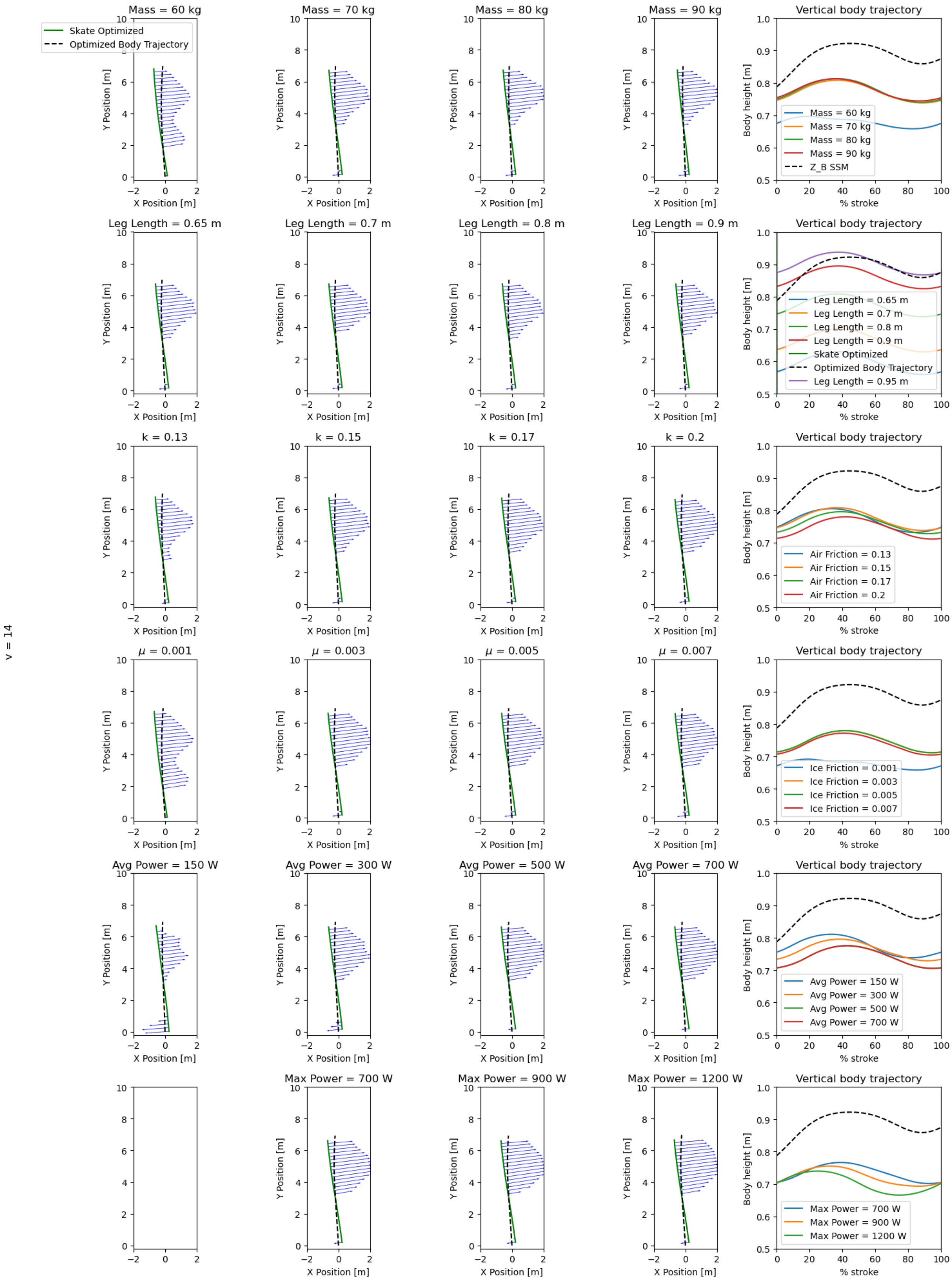

Fig. 24: Results of the optimized trajectories and lateral force for different variables at a speed of 14 m/s

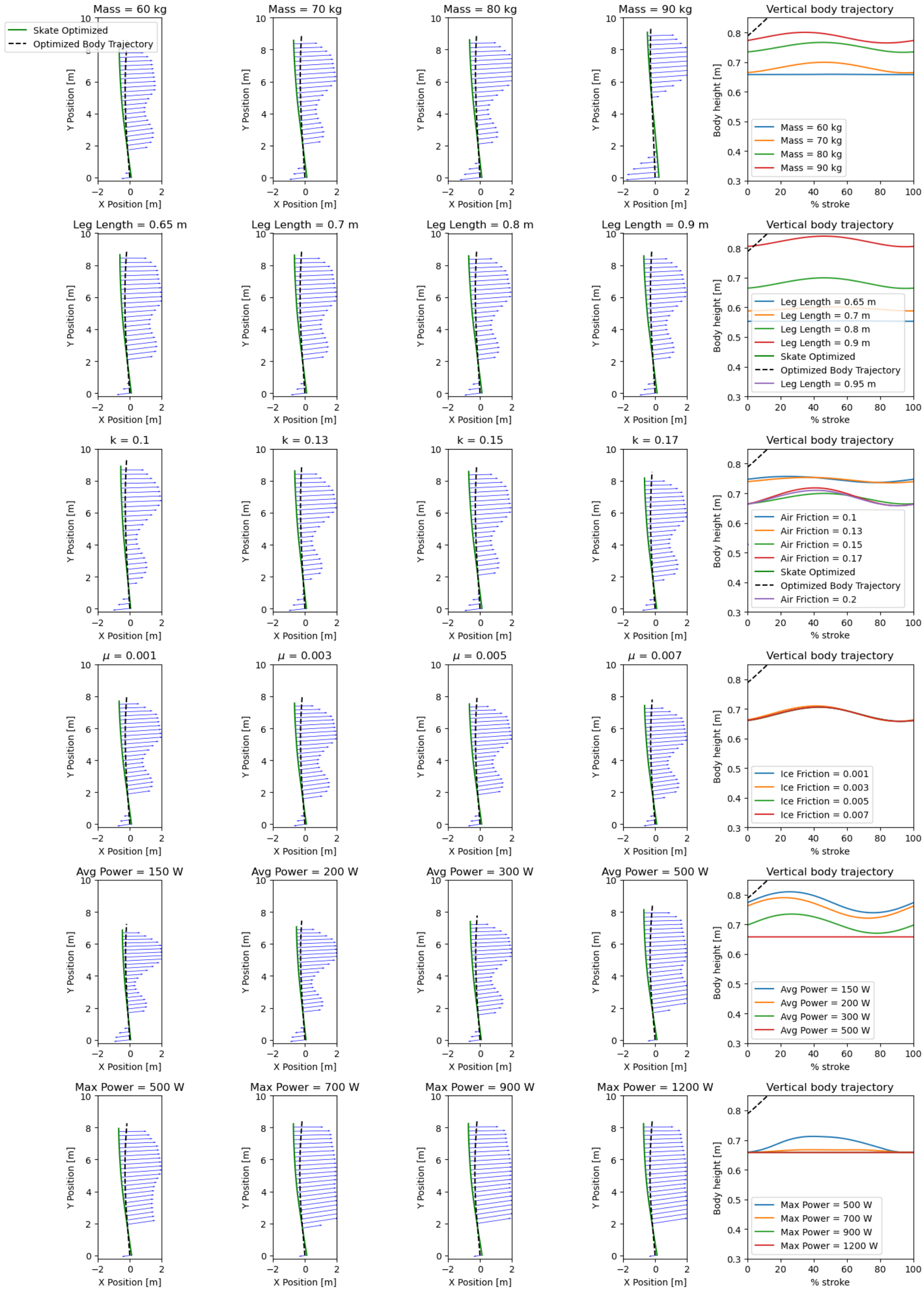

Fig. 25: Results of the optimized trajectories and lateral force for different variables optimized for maximal speed

APPENDIX J
PUSH-OFF MECHANICS FOR DIFFERENT TARGET SPEED UNDER VARYING CONDITIONS

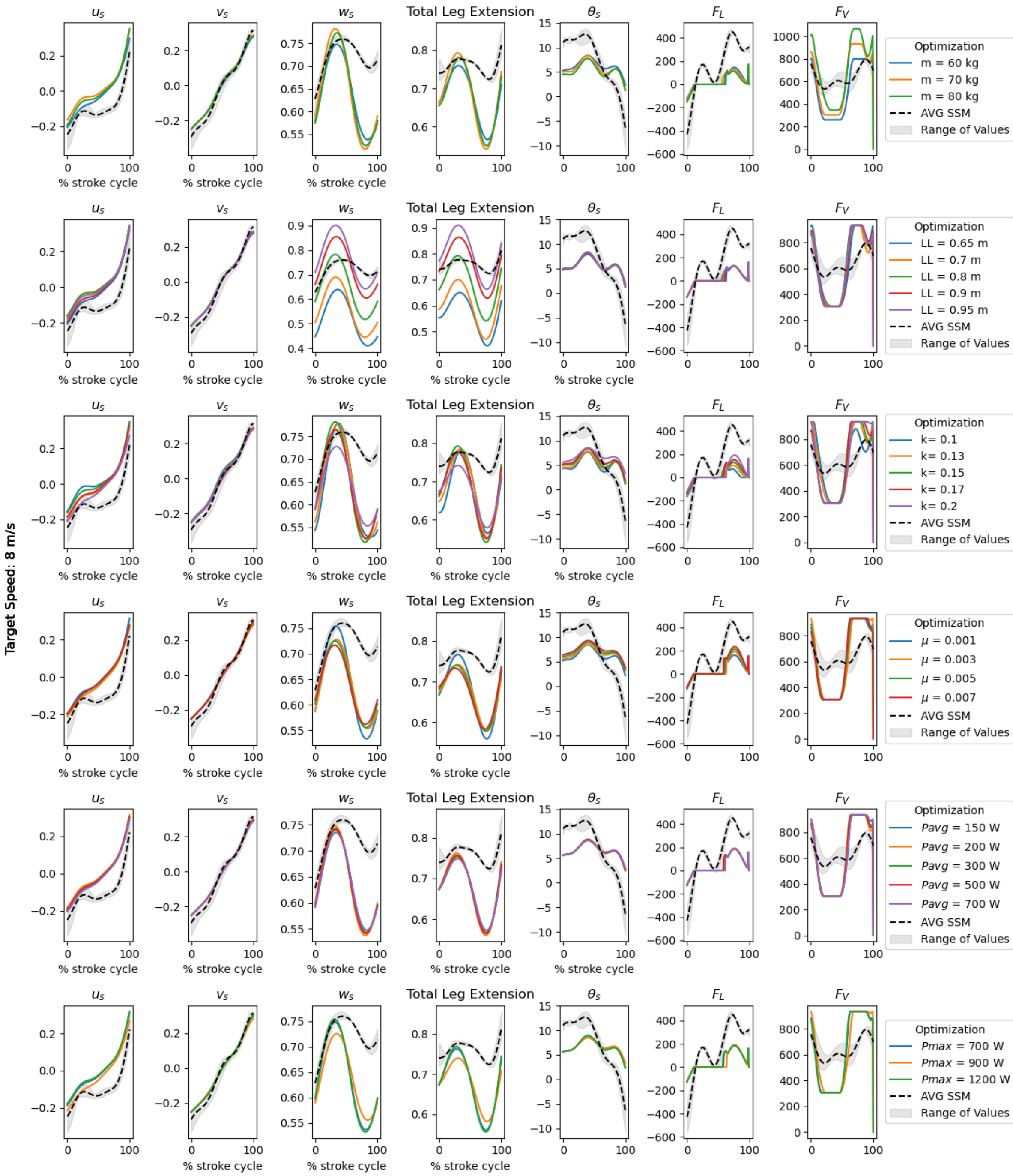

Fig. 26: Push-off mechanics for different variables at a speed of 8 m/s

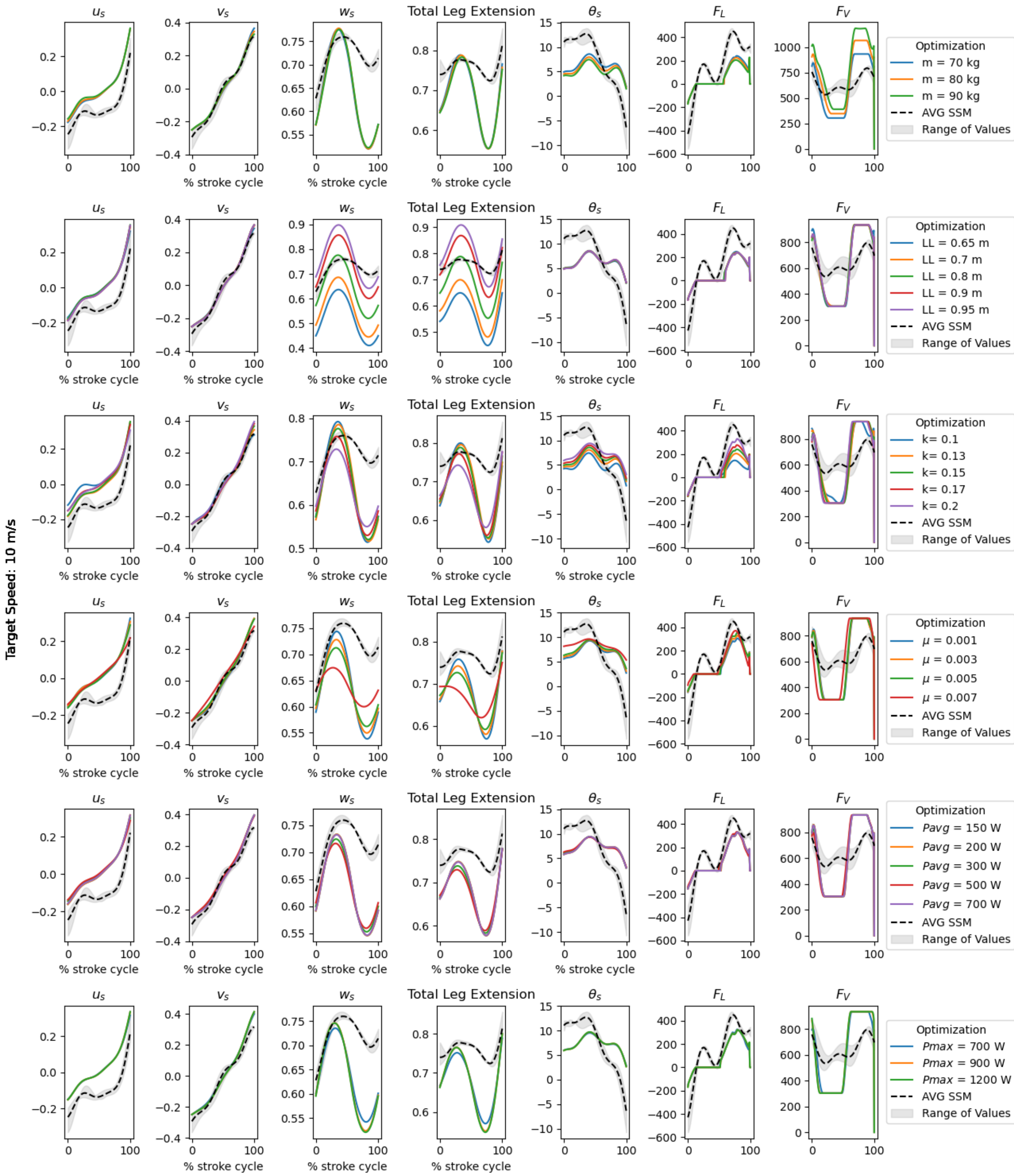

Fig. 27: Push-off mechanics for different variables at a speed of 10 m/s

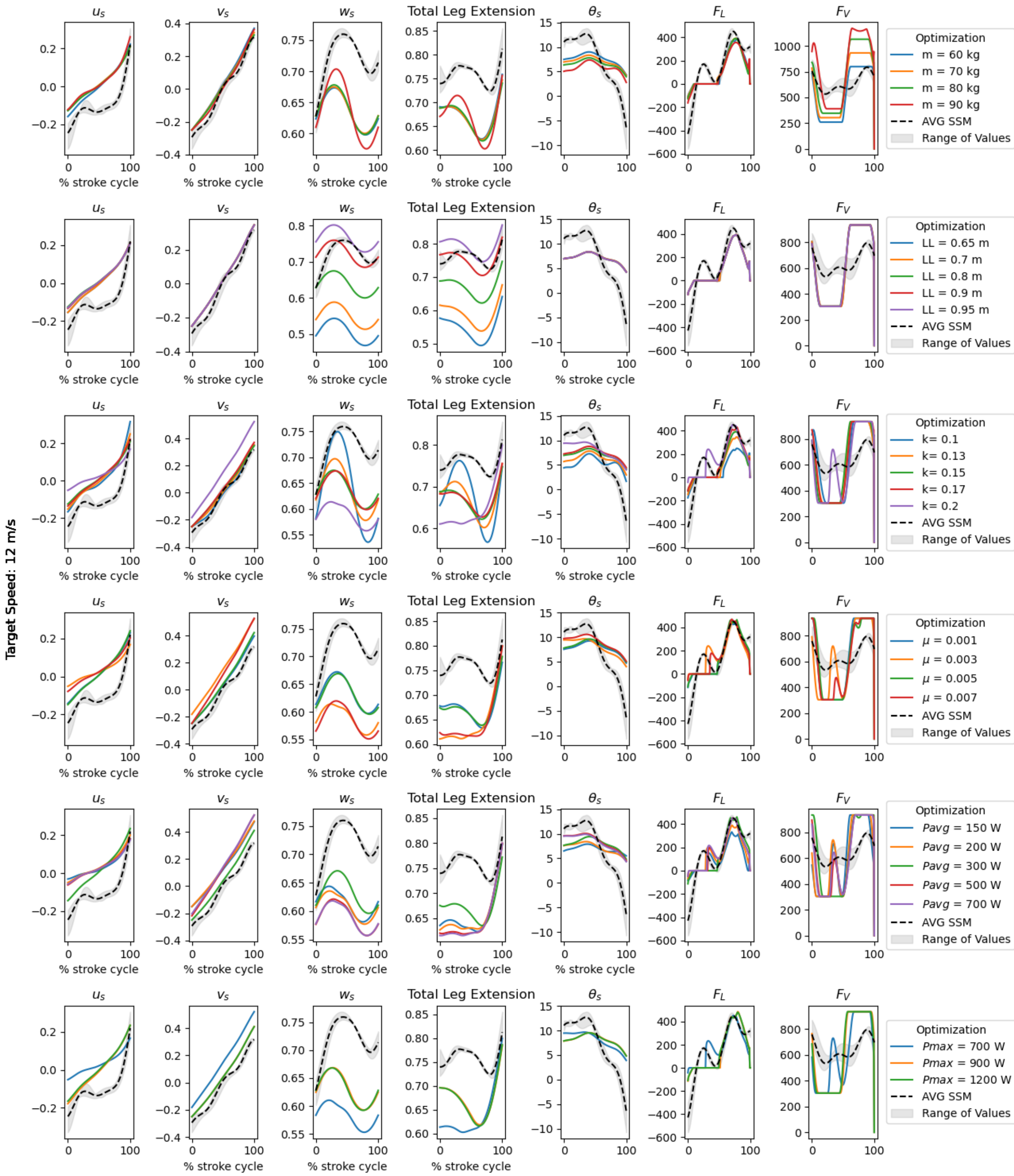

Fig. 28: Push-off mechanics for different variables at a speed of 12 m/s

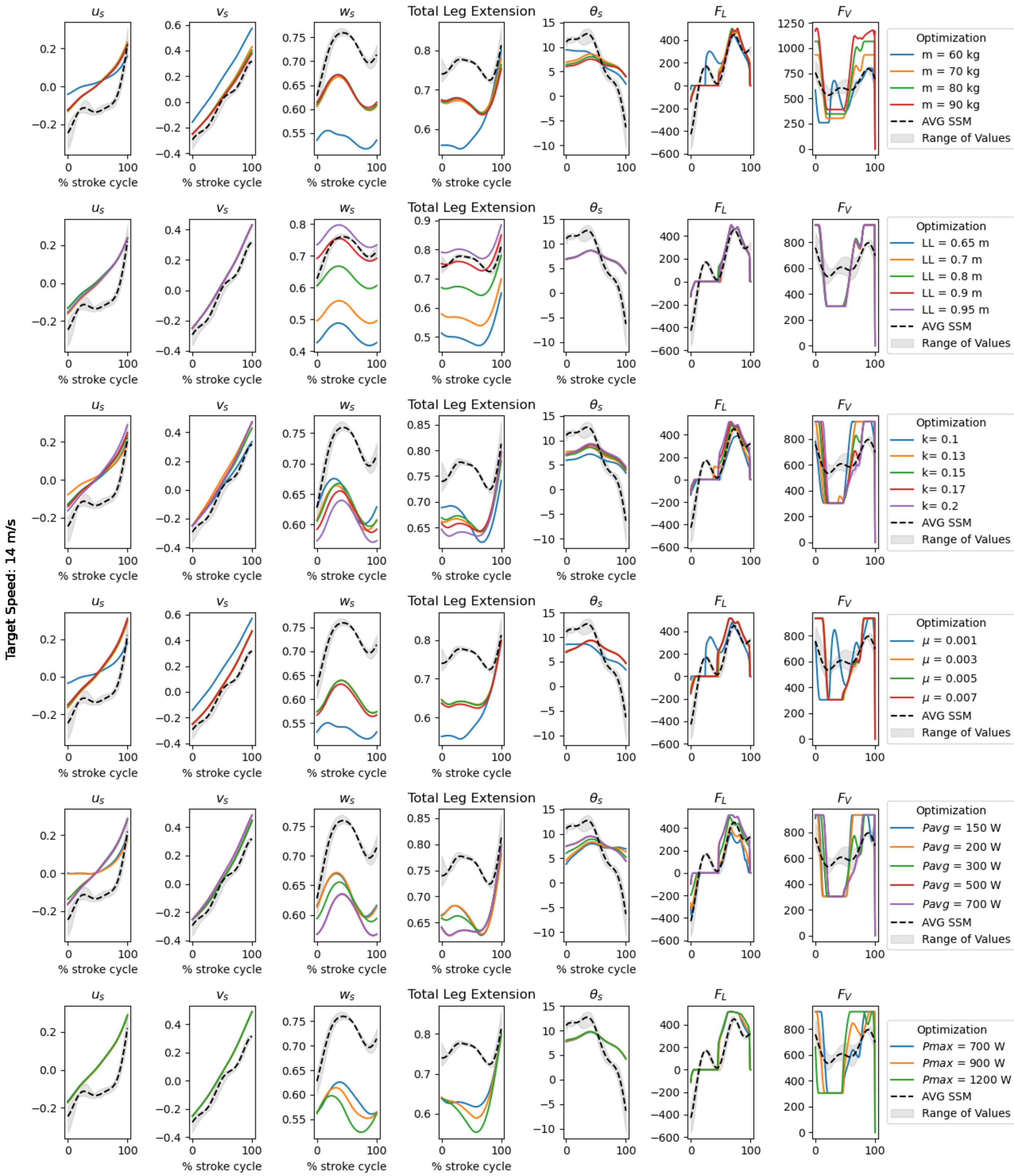

Fig. 29: Push-off mechanics for different variables at a speed of 14 m/s

APPENDIX K
PUSH-OFF MECHANICS WHEN MAXIMIZING SPEED FOR DIFFERENT VARIABLES

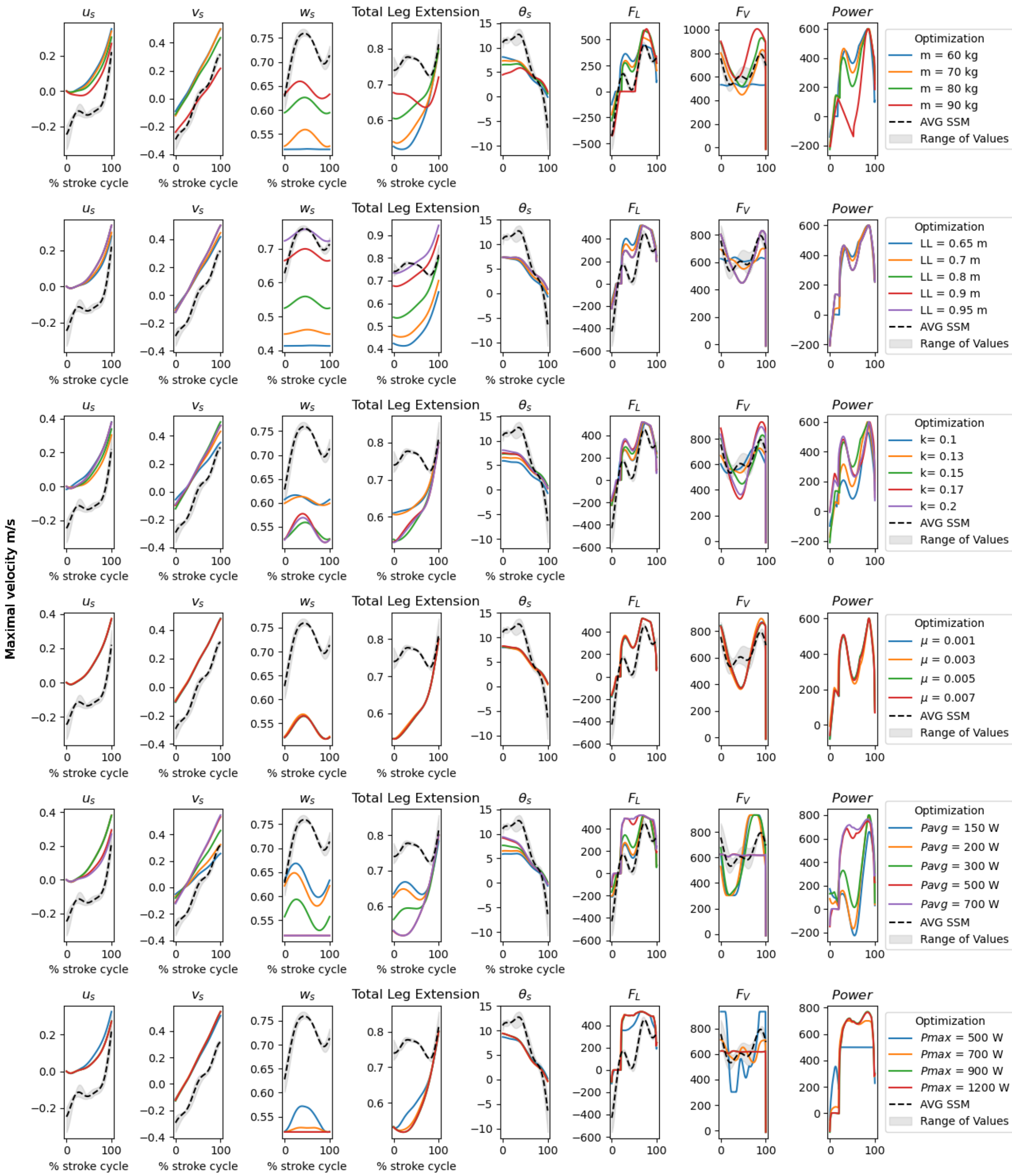

Fig. 30: Push-off mechanics for different variables when maximizing speed

Appendix L
Leg extension velocities for different frequencies

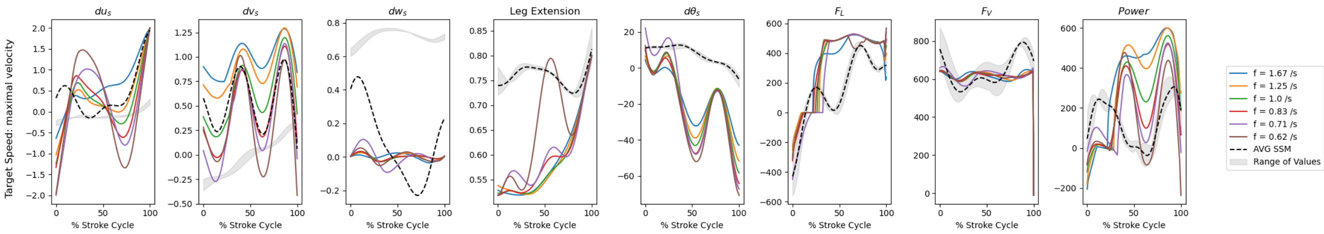

Fig. 31: Leg extension velocities for different frequencies, showing higher velocities for higher frequencies, especially in the sideways direction dv_s

Appendix M
Additional analysis second push

The aim of this additional analysis was to check the resulting skate trajectory and push-off forces, when the lateral force in the optimization was constrained to be larger or equal to zero ($F_L > 0$). This constraint prevents a double push-off technique. The total push-off forces are almost equal, but are slightly higher for the case with a second push. Power is slightly higher for the second push as well. The reason the optimizer converges to this solution is probably because this will reduce the penalty for deviating from the measured forces.

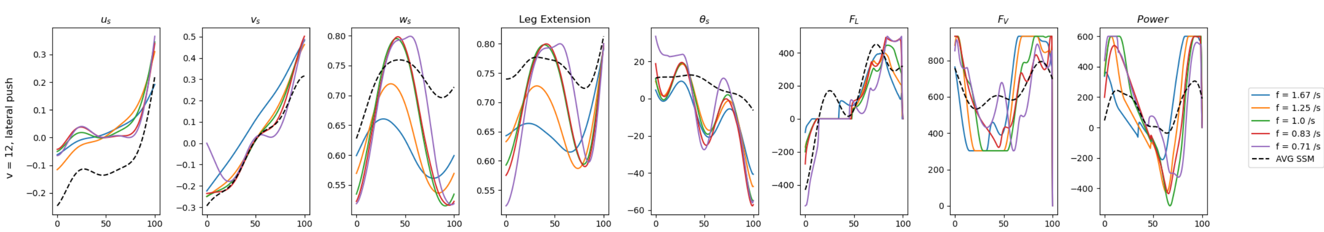

(a)

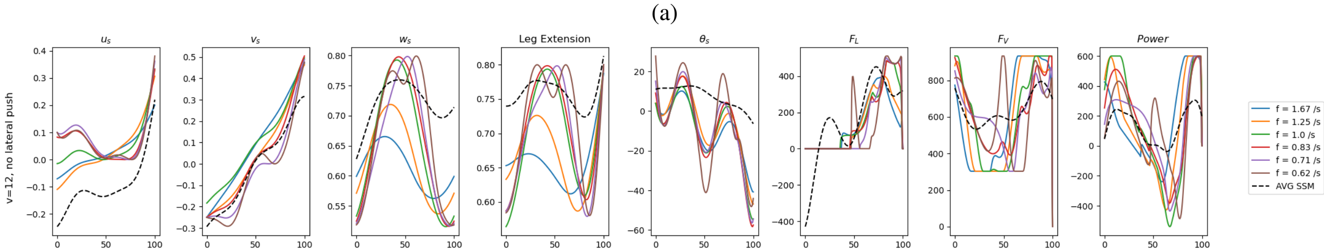

(b)

Fig. 32: This figure shows the difference in push-off mechanics when a secondary push at the beginning is not constrained (a), versus when it is constrained (b). Total forces were almost equal, just as the power, but slightly higher for the case where the double push was not constrained.

APPENDIX N
ADDITIONAL ANALYSIS GLIDING PHASE

As in the measured data, there constantly is a lateral force, concerns about the potential impact on stability and technique of a zero lateral push-off force during the gliding phase were raised. To address this, a secondary optimization was conducted to penalize extended periods of minimal lateral force. In this analysis, a penalty was added for low lateral forces. A large lateral force will cause an almost zero penalty, whereas the penalty will be large for really small lateral forces. This will encourage the model to find a solution that doesn't have the zero force gliding phase.

$$J_{penalty} = \frac{1}{F_L^2 + e^{-6}} \tag{53}$$

These results show higher forces when the gliding phase is penalized, explaining why the optimization is converging to a solution with a long gliding phase.

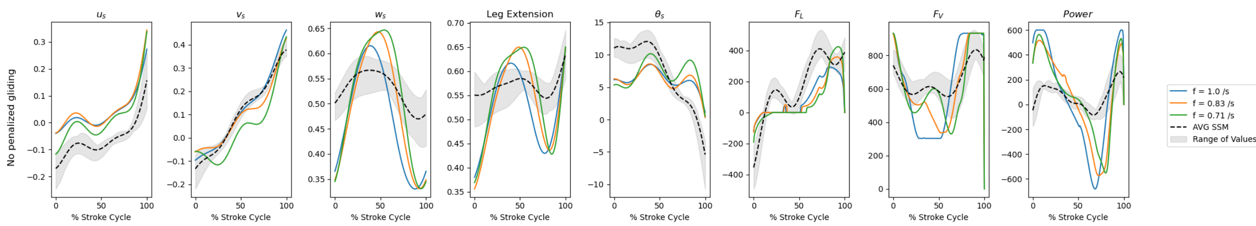

(a)

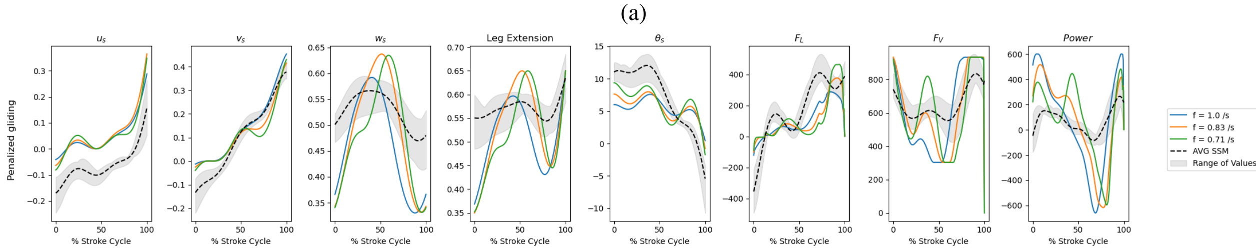

(b)

Fig. 33: (a) No Penalty. (b) Penalized gliding phase

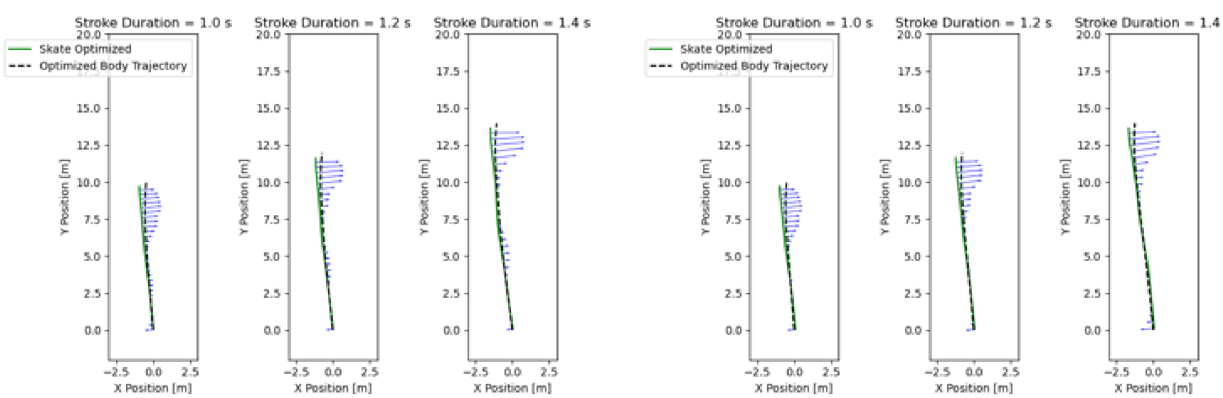

Fig. 34: The trajectory for penalizing no lateral force (left) vs without this penalty (right)